Visualization of Macromolecules—A First Step to Manipulation and Controlled Response

Sergei S. Sheiko* and Martin Möller*

Laboratory of Organic and Macromolecular Chemistry, University of Ulm, D-89069 Ulm, Germany

Received July 12, 2001

Contents

1. Introduction

The size and complexity of the structure of macromolecules allows the combination of different, in some cases even antagonistic, properties, e.g., in solubility, in flexibility, or electronic properties. The control of the connectivity of the molecular subunits can be used to transform short-range interactions into complex long-range structural organization. The examples of biomacromolecules demonstrate how single polymer molecules and their ensembles can serve as functional nanoobjects. While functional properties such as catalytic activity, directed motion, and the energy transport are well established in the case of biomolecules,[1−7] our ability to develop synthetic molecular devices is in its infancy. Significant efforts are directed toward shape control and directed motion.[8−14]

A major basis for the advancement in macromolecular functionality is our improving ability to control the macromolecular and supramolecular structures in great detail. Dense and cascade-type branching provided access to three-dimensional molecules, which do not interpenetrate but interact via their surfaces. Recent synthetic developments include microgels,[15−17] dendrimers,[18−26] and arborescent graft polymers.[27−31] Polymerization of substituted monomers as well as graft polymerization from a linear chain can yield cylindrically shaped macromolecules such as "hairy rods",[32,33] wormlike brushes,[34−40] and monodendron-jacketed chains.[41−46] The advancement in the control of the primary molecular structure and the manipulation techniques of the molecular conformation of such hyperbranched molecules make them intriguing building units for nanoscopic devices, biochemical sensors, molecular containers, templates for nanolithography, energy transfer funnels, and polyfunctional initiators and catalysts.[47−63]

Shape control and the development of shape-responsive molecules relies also on the availability of analytical tools that provide spatial resolution down to subnanometer scale, strong contrast with respect to the chemical composition and physical properties, sensitivity to molecular forces in the pN range, and in-situ monitoring of molecular motion and conformation with a time resolution down to and even below milliseconds.

Molecular probes, such as optical or magnetic tweezers,[64−71] micropipets,[72] and microfibers,[73,74] have been developed to manipulate single molecules and to measure their response to mechanical actions such as stretching, torsion, and compression. A force resolution down to 0.1 pN enabled quantitative measurement of the molecular forces and provided novel information on the basic principles of folding, motion, and interactions of individual molecules. Complementary to the local mechanical probes, actions of external fields were monitored on individual polymer molecules.[75−77]

Scanning probe microscopy, SPM, enables both visualization of single molecules[78−84] and probing of their properties.[85−94] In contrast to scanning tunneling microscopy (STM) that is limited to imaging of conductive materials,[95] scanning force microscopy (SFM) became a versatile method for characterization of the microstructure of polymeric materials at the nanometer scale.[96] In addition to the topological resolution, SFM can distinguish surface areas differing in local mechanical properties and composition, respectively.[101−103] Mechanical properties, such as viscoelasticity, friction, and adhesion, as well as long-range electrostatic and steric forces can be characterized on the scale of a few nanometers.[104−109]

SFM does not require any sample treatment like etching and metal sputtering but can visualize the native structure of the sample.[97−100] SFM is, however,

10.1021/cr990129v CCC: $36.00
Published on Web 12/12/2001

Sergei S. Sheiko was born in Moscow, Russia, in 1963. He received his B.A. degree in Physics from the Moscow Physico-Technical Institute in 1986 and his Ph.D. degree in Physical Sciences with Eduard Oleynik from the Institute of Chemical Physics of the Russian Academy of Sciences in 1990. From 1991 to 2000, he was working with Martin Möller at the University of Twente, Netherlands, and later at the University of Ulm, Germany. In 2001, he completed his Habilitation in Macromolecular Chemistry and joined the Department of Chemistry of the University of North Carolina at Chapel Hill. His main research interests include wetting and ordering phenomena in thin polymer films and functional properties of individual macromolecules.

Martin Möller studied chemistry at the University of Hamburg and Freiburg and then completed his Ph.D. degree at the Institute of Macromolecular Chemistry under the direction of Hans-Joachim Cantow on the microstructure of amorphous and semicrystalline polymers. He then worked with Robert Lenz at the University of Massachusetts on ionic blockcopolymers. In 1982 he returned to Freiburg, where he studied the structure and dynamics of crystalline and columnar flexible polymers by high-resolution-solid-state NMR techniques. In 1989 he moved to the University of Twente in the Netherlands, where he became professor of macromolecular materials and polymer technology. Then in 1993 he joined the University of Ulm as Professor of organic and macromolecular chemistry. His current interests regard the synthesis and structure–property relationships in branched and hyperbranched polymers, blockcopolymers, surface modification, self-organization of polymers in the bulk and in thin films, and the formation of functional nanostructures.

a contact method, and therefore, deformation of molecules due to contact with the probe is inevitable. Imaging of molecular details requires a sufficient fixation of the molecules so they do not get moved during scanning. Thus, SFM can provide a superior resolution and visualization of the molecular shape in the range below 100 nm at ambient conditions, however, with the handicap that the molecules are constrained to a 2D conformation by the necessary fixation on the support.

Biological macromolecules such as DNA represent prominent examples for SFM studies on single molecules.[79,110−118] Different techniques and deposition protocols have been reported to attach DNA molecules to a solid substrate and thus enable their imaging under water as well as in air. Strong electrostatic binding to the surface allowed DNA molecules to be scanned for long periods of time without damage and displacement. Imaging possibilities have been enhanced significantly with the introduction of the intermittent contact modes, since lateral forces were removed and perpendicular forces were reduced considerably due to higher sensitivity of the amplitude to the force variations.[108,109,119−121] At present, the local sensitivity of intermittent contact SFM to surface interactions and mechanical properties, in combination with a sharp tip, controlled humidity, and strong attachment to the substrate, enables stable and reliable imaging of the microstructure and the chemical composition of single molecules with a resolution down to 1 nm. Here, SFM is complementary to fluorescent microscopy, which allows observation of single biomolecules that are labeled with a fluorophore in a bulk solution but with a resolution larger than 100 nm.[123−130]

Recently, single chains of synthetic polymers have been visualized and examined regarding their conformation.[79−81,131−133] Mostly these were molecules with a well defined rather invariant shape like fullerenes, carbon nanotubes, and some polymer molecules. In this review we will focus on less rigid or even soft hyperbranched polymer molecules (Figure 1): (i) their visualization followed by analysis of the conformation and motion and (ii) probing of their properties such as specific interactions and mechanical properties. For comparison, some relevant examples from biomacromolecules are discussed.

2. Structure of Individual Molecules at Interfaces

2.1. Conformation of 2D Confined Macromolecules

So far, high-resolution microscopy can depict the contour of a macromolecule but does not resolve the individual atoms of a macromolecule. The information on the molecular structure obtainable from such an image includes the contour length, the curvature, and the end-to-end distance. This enables quantitative analysis both of the local properties (chain configuration and flexibility) and of the overall conformation (excluded volume effects and random-walk statistics). For polymer chains with a rodlike backbone or polymer molecules whose secondary structure is straightened by hydrogen bonds between the constituting monomers, e.g., DNA and proteins, the observed length L is directly related to its degree of polymerization, N, or its molecular mass M by the length per monomer unit $l_m = L/N$, and the linear density $\lambda = M/L$, respectively.

Figure 2 shows an SFM image of poly(isocyano-L-Alanine L-Alanine-OMe) (L,L-PIAA), that adopts a rigid-rod-like helix conformation stabilized by β-sheet-like hydrogen bonding between the alanine side chains.[131] Comparison of the number-average molec-

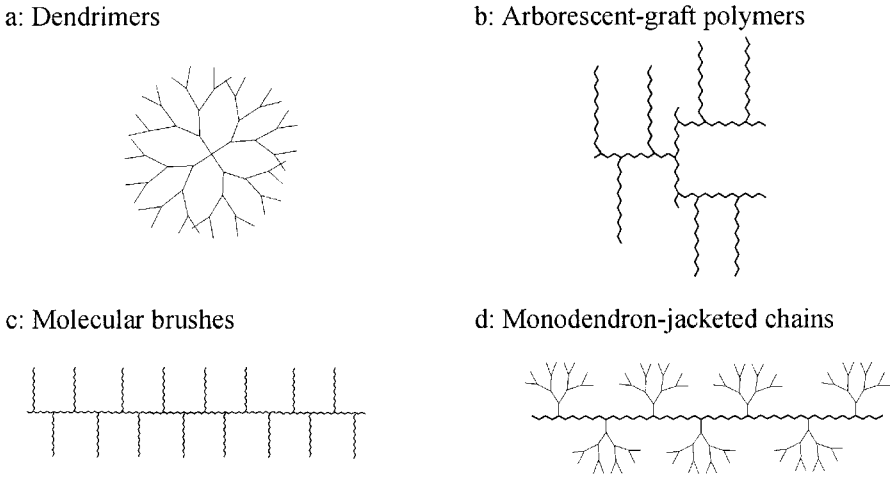

Figure 1. Hyperbranched molecular architectures.

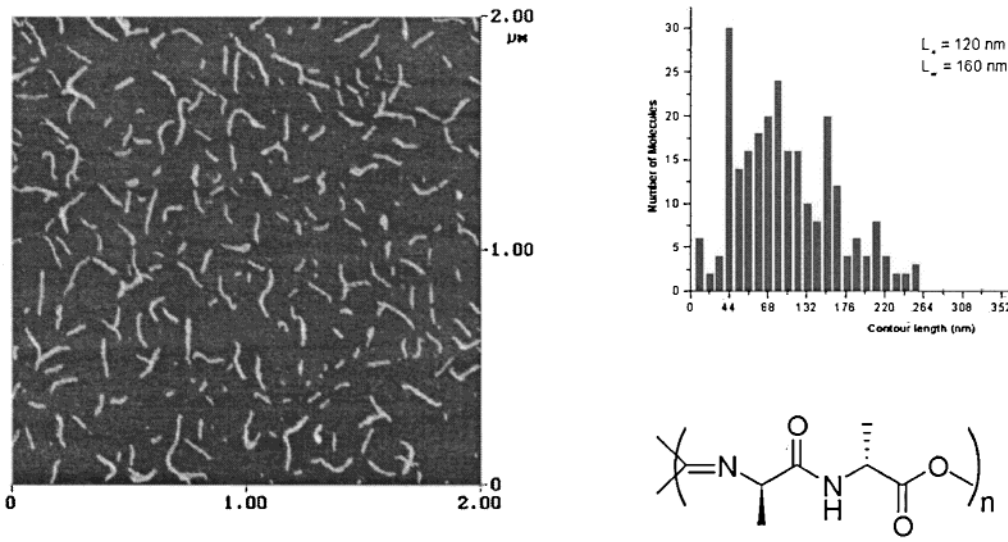

Figure 2. Height image of L,L-PIAA molecules on mica as measured by tapping mode SFM. The histogram shows distribution of the apparent lengths of the adsorbed molecules.

ular weight $M_n = 150$ kg/mol ($M_w/M_n = 1.4$) and the observed length of the molecules yields a length per monomer unit of $l_m \sim 0.1$ nm, which is consistent with the helical structure.

The local curvature, ρ, and the end-to-end distance, $\langle R_0^2 \rangle$, of disordered macromolecules reflect the chain flexibility and the long-range interactions, which on the other hand control macroscopic properties such as the viscosity of a polymer solution and melts. The description of the corresponding interdependences is usually done by means of scaling relations, the analysis of a polymer property as a power of polymer length, i.e., Property $\sim N^{\alpha}$.[134] Figure 3 depicts a schematic drawing of a wormlike molecule confined to a flat surface. The molecular flexibility, i.e., resistance to in-plane bending, can be characterized by the persistence length.[135] In an unperturbed state, the persistence length of a 2D-confined polymer chain should be 2 times longer than in a 3D system, i.e., in bulk or solution at the Θ temperature.[135−137]

Experimentally, one can use two complementary ways to evaluate the persistence length from the images of the chains. The bond-correlation function

$$\langle \cos(\Theta) \rangle = e^{-l/l_p} \qquad (1)$$

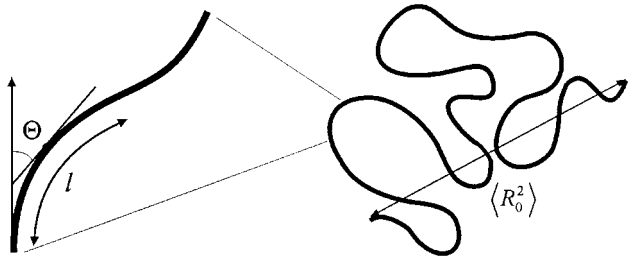

Figure 3. Molecular parameters which became accessible upon visualization of single molecules, i.e., contour length L, the end-to-end distance $\langle R_0^2 \rangle$, and the local curvature $\rho = d\Theta/dl$.

gives the average cosine angle between the tangents along the brush molecule separated by distance l. The characteristic length l_p corresponds to the persistence length. Since the method evaluates the local curvature, it can be applied to molecules of either length. The second method is based on the Kratky−Porod formula,[138] which depicts the dependence between the end-to-end distance $\langle R_0^2 \rangle$, the contour length L, and

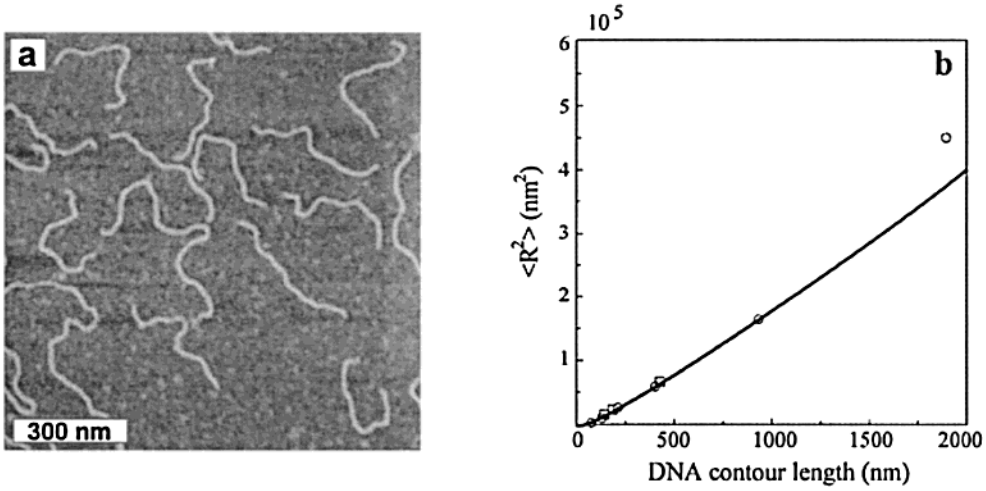

Figure 4. (a) SF micrograph of DNA molecules deposited on mica from a physiological solution. (b) Mean-square end-to-end distance, $\langle R^2 \rangle$, as a function of the DNA contour length measured in different buffer solutions. The continuous line represents the $\langle R^2 \rangle$ evaluated from eq 2 for a DNA persistent length of 53 nm.[79]

the persistent length as

$$\langle R_0^2 \rangle = 2 l_p L \left[1 - \frac{l_p}{L} (1 - e^{-L/l_p}) \right] \qquad (2)$$

The Kratky−Porod formula may be not applicable for long molecules with $L \gg l_p$, for which excluded volume interactions should be taken into account. Intramolecular excluded volume effects result from repulsion between segments within the same molecule, which can cause an increase of the end-to-end distance. These effects are particularly strong for 2D systems, which demonstrate an increased density of segments and do not permit the chain crossings. Both methods require complete visualization of a statistical ensemble of single molecules in order to determine the length L, the angle Θ, and the end-to-end distance $\langle R_0^2 \rangle$. In addition, they assume the observation of molecules in their natural state, in which molecules are not constrained and freely fluctuate around their equilibrium conformation.

The concurrent effects of adsorption, solvent evaporation, and capillary forces can, however, lead to kinetically trapped conformations (see below). The question arises whether and under what conditions an equilibrium 2D conformation can be achieved.

Optimum conditions were reported for DNA molecules deposited on mica.[78] In water, mica is negatively charged; and therefore, mica repels negatively charged DNA molecules. When divalent cations, such as Mg^{2+}, Mn^{2+}, Co^{2+}, and Ca^{2+}, are adsorbed, the surface charge is inverted. Thus, DNA adhesion can be promoted if deposition is done from a buffer solution containing divalent cations.[108] Because the divalent cations and thus the adhesion sites can diffuse along the surface, the deposition process was assumed to allow equilibration rather than being dominated by kinetic trapping effects. A typical example is a 0.5 nM DNA solution in a pH 7.4 buffer with NaCl (10 mM) and $MgCl_2$ (2 mM). In this case, the adsorption of DNA molecules from solution is controlled by diffusion. A diffusion coefficient of $D = 5.5 \times 10^{-8}$ cm^2/s was found using the formula $n_s/n_0 = \sqrt{4D/\pi}\sqrt{t}$, where n_s is the surface concentration of the adsorbed molecules and n_0 the concentration of the molecules in solution.

At low concentrations from 0.5 to 2 nM, the molecules are adsorbed onto mica as single species as shown in Figure 4a. Figure 4b shows a plot of $\langle R_0^2 \rangle$ as a function of the contour length L. Both parameters were measured directly from the SFM micrographs. Assuming that the molecular conformation was not perturbed by excluded volume interactions between molecular segments as well as by interactions between the segments and the substrate, Rivetti et al. used the Kratky−Porod formula to determine a persistence length of 53 nm.[79] The data were in good agreement with those obtained by electron microscopy and gel electrophoresis.[139] For the molecules adsorbed on mica, the crossover of the perturbed and unperturbed regimes was found at contour lengths of about 1000 nm (ca. 20 times the persistence length). Therefore, evaluation by the Kratky−Porod formula (eq 2) is limited to DNA molecules whose length is shorter than 1000 nm.

The effect of excluded volume repulsion on the molecular conformation was investigated for long DNA molecules in an aqueous environment by fluorescence optical microscopy. Figure 5a shows fluorescence images of λ-phage DNA fragments bound to a glass-supported cationic lipid membrane in 10 mM HEPES buffer. Since the observed molecules were much longer than the persistence length, the excluded volume effects resulted in the coil expansion. Figure 5b depicts the log−log representation of the radius of gyration as a function of the number of base pairs for a set of molecules that consist of 880, 6141, 14 953, and 26 528 base pairs.[140] The scaling exponent for the 2D-confined molecules was found to be $\nu = 0.79 \pm 0.04$. This experimental value is in good agreement with the theoretical prediction $\nu = 3/4$ for self-avoiding statistical chains in two dimensions[141] and consistent with a persistence length l_p of 50 nm. For individual DNA molecules in solution, the scaling exponent was determined to $\nu = 3/5$.[142]

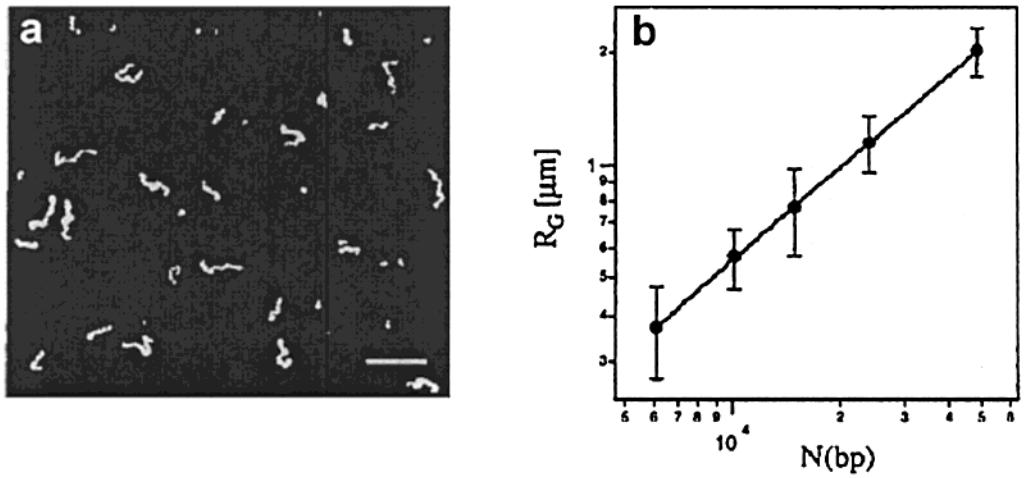

Figure 5. Static scaling analysis of single DNA molecules. (a) Fluorescence micrograph of λ-phage DNA cut by the restriction enzyme BbrPI. (b) The log−log plot of the averaged radius of gyration of DNA fragments as a function of fragment length in number of base pairs N(bp). The straight line fits the scaling $R_g \propto N^{\nu}$, with $\nu = 0.79 \pm 0.04$.[140]

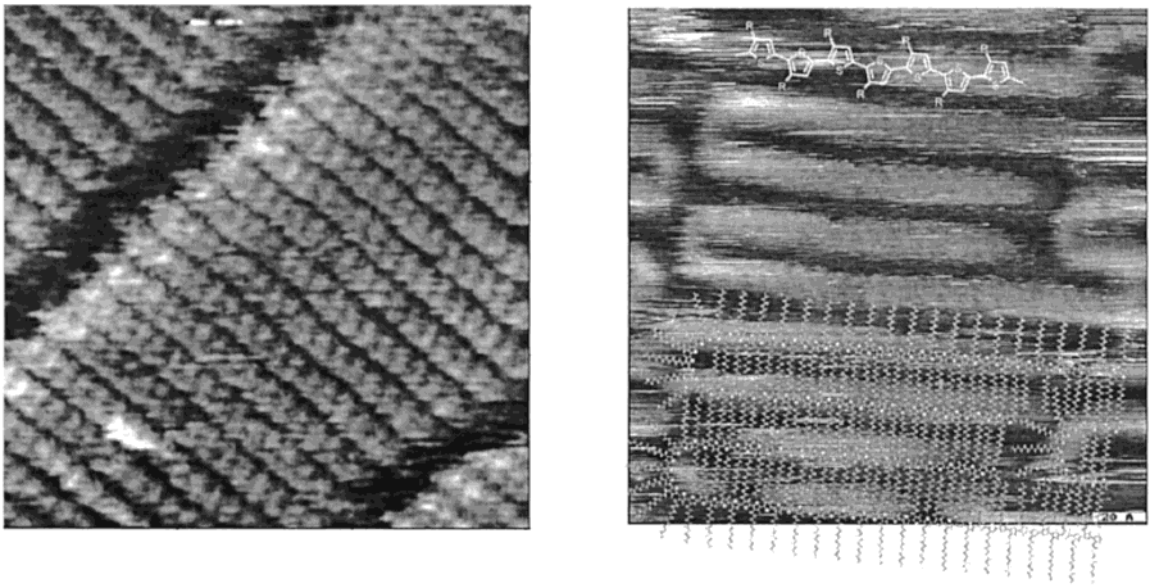

Figure 6. (a) STM image of C36H74 alkane on graphite.[143] (b) Head-to-tail-coupled poly(3-dodecylthiophene) in the HOPG/liquid (1,2,4-trichlorobenzene) interface 20 × 20 nm.[145]

2.2. Structural Effects by Specific Interactions with the Substrate

Absence of surface interactions that effect the conformation of the macromolecules is, however, not the rule. Below we will discuss examples of how the molecular conformation can be effected by specific interaction with the substrate. Obviously, one cannot regard the apparent persistence length of the adsorbed molecules as a characteristic value for the chain flexibility.

Spectacular pictures of adsorbed chain molecules have been obtained for *n*-alkanes on graphite where the carbon chains were oriented according to the 3-fold symmetry of the graphite (Figure 6a). The orientation of the main chain has been explained by the close matching between the repeat length l_e = 2.54 Å of a $-(CH_2-CH_2)-$ sequence in all-trans planar zigzag conformation and the crystallographic spacing a = 2.46 Å of the graphite surface.[143,144]

Also, interactions of the side chains with the substrate can cause alignment of adsorbed molecules. Figure 6b shows the ordering of polythiophene molecules with alkyl side chains along the crystallographic axes of the graphite.[145] Formation of highly ordered monolayers follows from the epitaxial-like orientation of the hydrocarbon chains with respect to the graphite lattice.

Also, relatively long polymer molecules can be extended and aligned by specific adsorption of the side groups with the substrate. Detailed studies of the molecular conformation affected by adsorption on a solid substrate have been possible with so-called monodendron-jacketed polymers.[41,146−148] Scheme 1 depicts two examples of monodendron-jacketed macromolecules: 14-ABG-PS carries three monoalkoxybenzyl ether groups per monomer unit, whereas the stronger branched 3,4,5-t-3,4,5-PS monomer is substituted by three trisalkoxybenzyl ether groups and has a 2 times larger molecular mass.[149]

Figure 7 shows an SF micrograph of 14-ABG-PS on graphite together with a cartoon of the molecular structure.[147] The macromolecules are arranged in

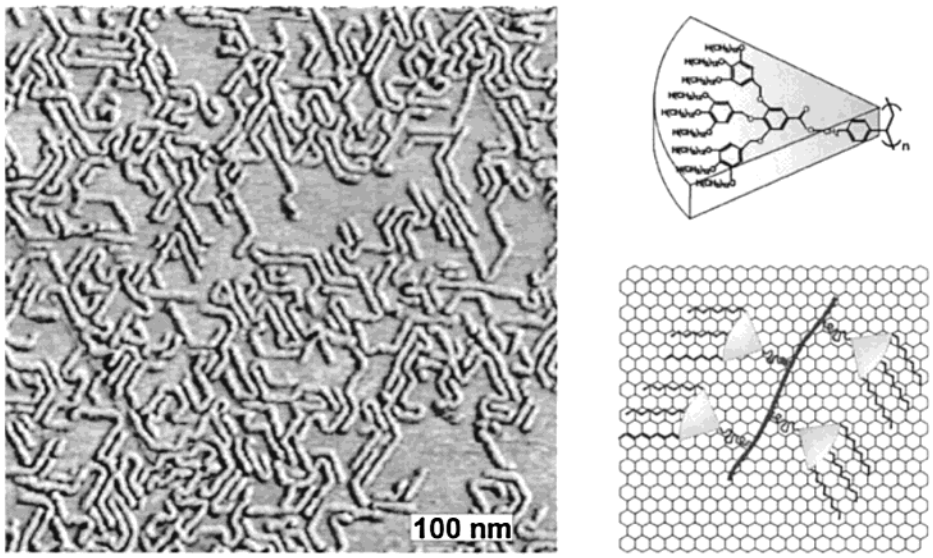

Figure 7. SFM micrograph of 14-ABG-PS molecules on HOPG prepared by spin casting of a solution in cyclopentane (c = 0.1 mg/mL). Individual molecules aligned parallel to the substrate and bent at characteristic angles of 60° and 120° to follow the 6-fold symmetry of graphite.[147]

Scheme 1

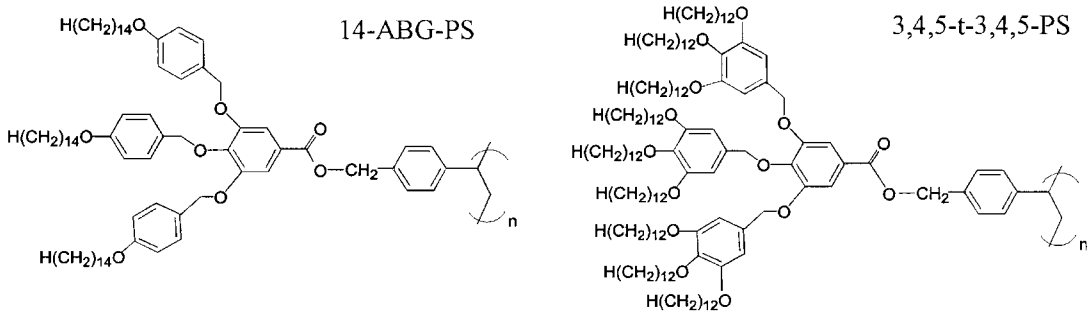

straight segments with bends of a characteristic angle of 60° and 120°. Also, in this case the ordering of the macromolecules is explained by an epitaxial adsorption of the alkyl tails of the monodendron side groups on highly oriented pyrolytic graphite, HOPG. Specific interaction of the side chains with the substrate has been verified by STM studies on monolayers of the monodendrons.[148]

It has also been possible to observe how the chains adsorb originally in a coiled conformation and how they expand subsequently to the ordered pattern. Figure 8 shows a series of SFM images of a polyoxnorbornene substituted by the same dendron groups as in the case of 14-ABG-PS after different times for adsorption.[148] Besides the increase in surface coverage, one observes the relaxation within minutes.

On mica, the 14-ABG-PS polymer did not show any particular order (Figure 9). Only a short-range orientational order of densely packed cylinders was observed.

The dense arrangement of the chains points to the action of other forces that can control the molecular conformation of adsorbed macromolecules in addition to the interaction with the substrate. Capillary forces and dewetting during evaporation of the solvent can cause condensation and dense packing of the molecules in monolayer patches,[147,148,150] For large molecules with a diameter of ca. 5 nm, capillary forces are in the range of a few nN, which is sufficient to move the molecules or molecular parts along the substrate and to cause aggregation of individual molecules into monolayers.

Another example for wormlike synthetic macromolecules is depicted in Figure 10. The SFM images show poly(methyl methacrylate) brush molecules that adsorbed as extended threats on a flat mica surface. The backbone consists of methacrylate units, each of which is grafted by a methyl methacrylate side chain.[151] The molecular properties are summarized in Table 1.

Neglecting the interaction with the substrate, the overall conformation of the brush molecule is controlled by the repulsion and excluded volume of the densely grafted side chains. Thus, the spatial demand of the side chains results in bending rigidity and prevents the collapse of a brush molecule to a dense globule. Yet, in contrast to DNA, where the segmental conformation, i.e., the rotational angles of the bonds in the backbone, is fixed to a large extent, the brush molecules possess a flexible backbone. Thus, the brush acquires rigidity on the length scale of it's thickness or larger, but the conformation within short segments of the backbone can be disordered similar to that in a coil molecule. The monodendron-jacketed polymers depicted in Figures 7−9 can be regarded as an intermediate case, where the rigidity of the backbone conformation is caused not only by the bulkiness but also by self-assembly of the side chains

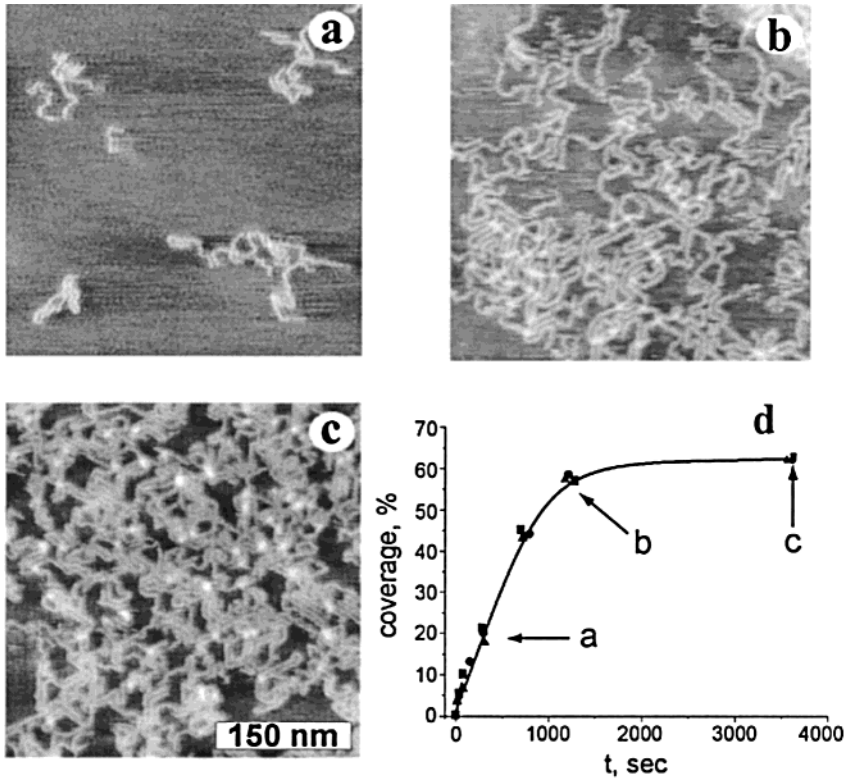

Figure 8. (a−c) A series of SFM micrographs was measured after adsorption of polyoxanorbornene DP100 from THF solution with concentration 0.001 mg/mL on mica during different times. The adsorption time is indicated by arrows in d, representing dependence of the coverage on the time for different polyoxanorbornenes (■) DP 100, (●) DP 200, (▲) DP 400.[148]

Table 1. Molecular Characterization of the PMMA Brushes Depicted in Figure 5[151]

length of side chains[a]	total molecular weight[b]	contour length (SFM)[c]	L_w/L_n	length/monomer (SFM)
2410 g/mol	1.08×10^{7} g/mol	367 nm	1.3	0.07 ± 0.1 nm

[a] MALDI-TOF. [b] Small angle light scattering. [c] $L_w = (\sum n_i L_i^2)/(\sum n_i L_i)$.

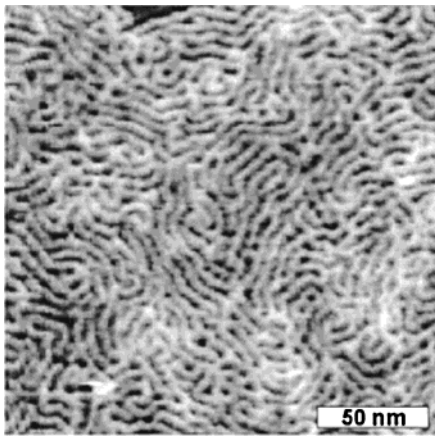

Figure 9. SFM micrographs of 14-ABG-PS molecules on mica deposited from a $CHCl_3$ solution (c = 0.1 mg/mL). Molecules are densely packed because of the action of capillary forces during evaporation of the solvent.[147]

with their π-stacking of the aromatic units. Yet, also in this case, the self-assembly to column structures does not prevent some randomness in the rotational isomeric states.[146,149] Because of this flexibility of the main chain, the brush and also mondendron-jacketed molecules can experience an axial contraction compared to the maximum contour length given for an all-trans planar zigzag conformation (2/1 helix).

A reduced length per monomer unit, i.e., of the effective grafting distance h, has been demonstrated for the PMMA brush molecules depicted in Figure 10. Comparison of the degree of polymerization of the PMMA brushes with their length determined by a detailed evaluation of a set of SFM images yielded a length per monomer unit of $h = 0.07 \pm 0.01$ nm. The value is 3 times shorter than the monomer length in a completely stretched backbone ($h_{\text{all-trans}} = 0.25$ nm).

Evaluation of the cross section of the brush molecules in Figure 10 (including correction for tip indentation[152] convolution of the surface profile with the shape of the tip apex and comparison with electron microscopy images) demonstrated that the molecules adopt a hemicircular cross section of 11 ± 1 nm width and a height of 4.2 ± 0.5 nm. These values are consistent with $h = 0.07 \pm 0.01$ nm for the length per repeat unit of the backbone, i.e., with the molecular weight of the side chains and the bulk density of PMMA, a length of 0.07 nm corresponds to a cylinder with a cross section of 45 nm^2, comparable to the cross section of 38 nm of a hemicircular profile with 11 nm width and 4.2 nm height.

Light scattering studies allowed a complementary characterization of the size and conformation of the

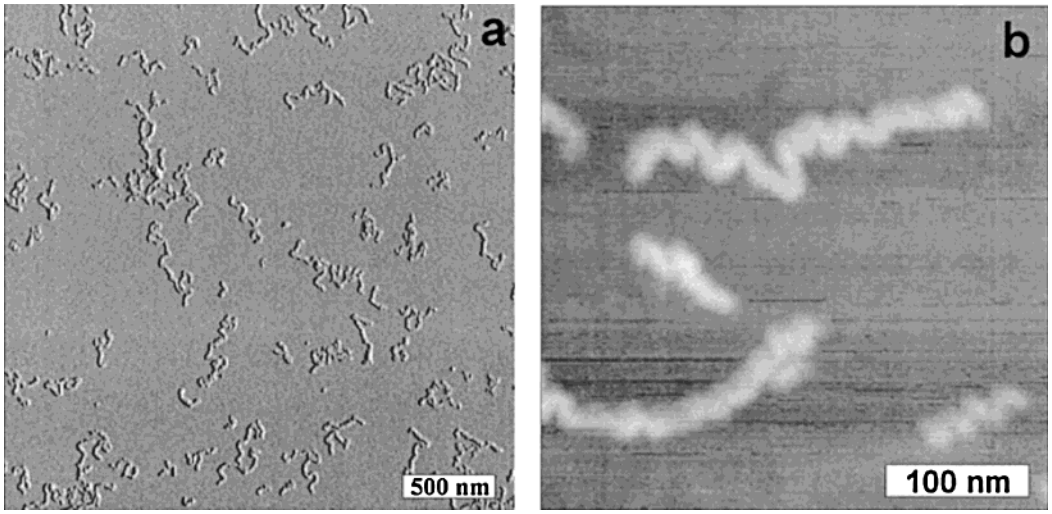

Figure 10. (a) Molecular brushes with poly(methyl methacrylate) side chains were adsorbed on mica and annealed above the glass transition temperature $T = 105$ °C for 24 h. (b) The undulated structures in higher magnification images demonstrate the tendency of the brush molecules to contraction via the buckling mechanism. The height of the molecules was determined to be 2 nm and the width 16 ± 2 nm.

PMMA brush molecules in THF solution.[151] Also, in this case, the monomer length $h = 0.081 \pm 0.008$ nm indicated an axial contraction compared to the fully stretched all-trans conformation. The coincidence of the experimentally determined values for h in dilute solution and for the dry adsorbed molecules might be regarded as an indication that the axial contraction of a densely grafted brush molecule does not depend strongly on the quality of the solvent. It must, however, be noted that adsorption of the side chains, i.e., their confinement to a 2D conformation, can cause significant stretching compared to the unconfined brush (see below). Thus, an axial contraction caused by decreasing solvent quality or in a dry brush might well be compensated by stretching due to partial adsorption of the side chains. That this is in fact the case is indicated by the remarkable buckling of the brush conformation observed in Figure 10b. Buckling can be explained by a transformation where the molecules first contract as the solvent evaporates and then expand axially as the side chains start to adsorb tightly. Buckling is typical for confined anisotropic systems when the strain cannot be released completely, such as thin films, microtubuli, and nanotubes.[153−155]

The driving force for the axial contraction was elucidated by O. Borisov by scaling analysis of a linear brush molecule.[156] Because of the dense substitution, the side chains get stretched. Stretching of the side chains with respect to the Gaussian dimension leads to conformational entropy loss. Thus, if the grafting density h^{-1} is fixed, the cylindrical brush experiences an extensional axial force of entropic origin. In a bad solvent or in air when the brush is collapsed, a negative contribution to the axial force has to be taken into account due to the excess interfacial energy of the brush. The interfacial energy per unit area is proportional to τ^2, where τ describes the quality of the solvent given by the relative deviation from the Θ point, $\tau = (T - \Theta)/\Theta$. The free energy per side chain, F, in a collapsed brush comprises the elastic penalty for extension of a side chain, the excess free energy of the interface, and the free energy of excluded volume interaction.[156−159]

$$\frac{F(R,h)}{k_B T} = \frac{R^2}{N} + |\tau|^2 Rh - |\tau|^2 N \qquad (3)$$

Here N is the number of monomer units in the side chains and R is their end-to-end distance. In a uniformly collapsed brush below the Θ point, the binary interactions are attractive and the polymers density $\propto |\tau|$. The thickness of the collapsed brush scales as $R \propto (N/h|\tau|)^{1/2}$. The axial tension is given by

$$f/k_B T = -\frac{\mathrm{d}F/k_B T}{\mathrm{d}h} \cong (|\tau|h^2)^{-1} - |\tau|^{3/2}(N/h)^{1/2} \qquad (4)$$

The degree of stretching of the side chains and the extensional force on the backbone decreases with decreasing grafting density and decreasing solvent qualityτ (i.e., increasing $|\tau|$).

If the backbone is not stiff but flexible, an eventually resulting negative axial tension can be partly released by contraction, i.e., variation of the effective grafting density h. Moreover, under the condition of a fixed monomer density $N/(R^2 h) \cong |\tau|$, minimization of the total elastic free energy of the collapsed brush has been shown to result to[156]

$$h(\tau) \cong h(\tau_\Theta(|\tau|/|\tau_\Theta|)^{-1/3}$$

$$R(\tau) \cong R(\tau_\Theta(|\tau|/|\tau_\Theta|)^{-1/3} \qquad (5)$$

with τ_Θ corresponding to the onset of the side chain collapse.

The detailed analysis[156] demonstrated that the onset of the side chain collapse is shifted toward the range of poorer solvent conditions compared to that in an individual chain of length N. Both the side chains and the backbone remain extended at $\tau \leq \tau_\Theta$ with respect to the Gaussian dimensions for densely grafted brushes, and the length of a dense brush is

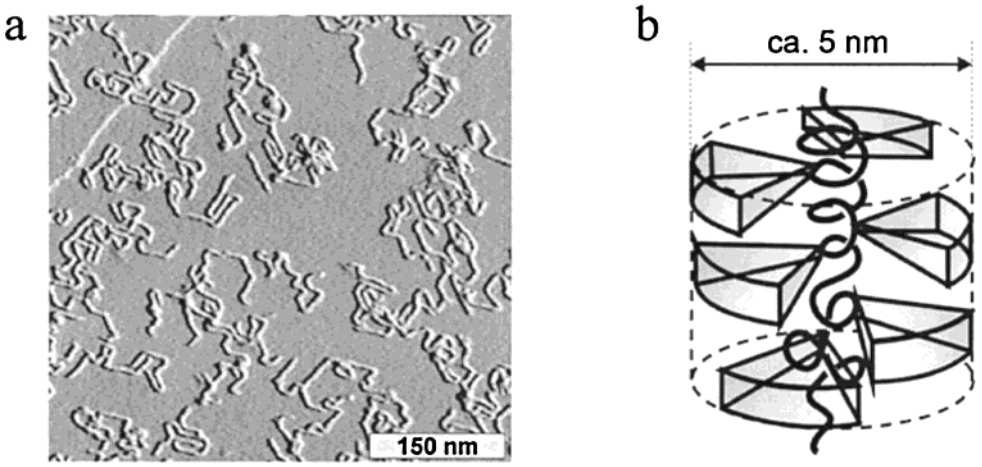

Figure 11. (a) SFM micrograph of single 14-ABG-PS molecules on HOPG, and (b) suggested conformation of monodendron-jacketed linear chains.[146]

Table 2. Molecular Dimensions and Length Per Monomer Unit of 14-ABG-PS, 3,4,5-t-3,4-PS, and 3,4,5-t-3,4,5-PS from SFM Micrographs and SEC and SLS Data[146,147]

	polymers		
	14-ABG-PS	3,4,5-t-3,4-PS	3,4,5-t-3,4,5-PS
M,[a] g/mol	1194	1612	2140
M_w,[c] 10^6 g/mol	1.1	1.2	2.0
M_w/M_n	2.6	2.6	2.2
a,[c] Å	52.1	41.4	47.7
l_{XDR},[d] Å	0.8	1.8	2.0
l_{SFM},[e] Å	1.2	1.9	2.3

[a] Molecular weight of the monomer unit. [b] Molecular weight of the polymers determined by size exclusion chromatography in tetrahydrofuran using a light scattering detector. [c] Column diameter determined by X-ray diffraction measurement in the columnar mesophase. [d] X-ray spacing along the column axis per repeat unit of the main chain as determined for the columnar mesophase in bulk. [e] Length of the cylindrical molecules per repeat unit of the main chain determined from the SFM micrographs as $l_{SFM} = M \cdot L_n/M_n$.

predicted to depend only weakly on the solvent conditions within the regime of a poor solvent.

Also, in the case of the monodendron-jacketed macromolecules, the chain length-per-repeat unit $l_{SFM} = L_n/DP_n$ could be evaluated from the molecular length in comparison with the independently determined degree of polymerization DP_n. Figure 11 depicts an SFM image of single 14-ABG-PS molecules deposited on the surface of highly oriented pyrolytic graphite.[146,147] The 5 nm thick molecular threads are aligned parallel to the substrate plane. Table 2 summarizes the molecular dimensions and the values of the length per monomer unit, l_{SFM}, for three monodendron-jacketed polystyrenes with three, six, and nine terminal alkyl chains per dendron, respectively.

The value of $l_{SFM} = 1.2$ Å for 14-ABG-PS is in good agreement with the stacking period in the columnar hexagonal mesophase that was obtained from the macroscopic density and the X-ray periodicity of the columnar packing. This value is almost 2 times less than the length $l_0 = 2.5$ Å expected for a fully extended main chain in an all-trans planar zigzag conformation. In contrast, 3,4,5-t-3,4,5-PS with the sterically more demanding side groups demonstrated almost complete stretching of the backbone with $l_{SFM} = 2.3$ Å.

Clearly, also the monodendron-jacketed polystyrenes are contracted in length compared to the full contour length. For 14-ABG-PS it must be noted, however, that the coincidence of the length per monomer unit in the adsorbed and the hexagonal columnar mesophase has to be considered to occur by chance. As discussed for Figure 7, the molecular conformation of 14-ABG-PS is significantly affected by the interaction with the substrate.[146−148] Certainly such an interaction with the substrate will be a factor that changes the segmental conformation and does not only align the molecular segments in a straight line. In this case, the length per monomer unit results from the interplay between the interfacial and intramolecular interactions. Constraint of the tightly adsorbed side chains to the surface plane causes extension of the backbone, while aggregation of desorbed side chains favors contraction.

2.3. Metastable Tertiary Structures by Local Contraction and Twisting

It is obvious that the conformation of adsorbed molecules can be far from equilibrium if the adsorption process has been fast and irreversible. In this case, the molecules do not have time to sample the whole assembly of thermodynamic states and get trapped kinetically at the contact sites. Yet, there are distinct kinetic pathways that give rise to the formation of peculiar tertiary structures in connection with the axial contraction and local twisting. An example discussed above is the buckling of the PMMA brushes in Figure 10. Another example is demonstrated in Figure 12. Here 14-ABG-PS molecules are depicted that were deposited by fast spin coating on mica.[147] The molecules were adsorbed randomly without interfacial ordering effects, and quick evaporation of the solvent caused underwinding or overwinding of the molecules, i.e., significant torsional strain is evidenced by the observation of supercoils, so-called plectonemes (from the Greek meaning "braided string").[161]

The drawing of a monodendron-jacketed chain in Figure 11 indicates that axial contraction is enabled

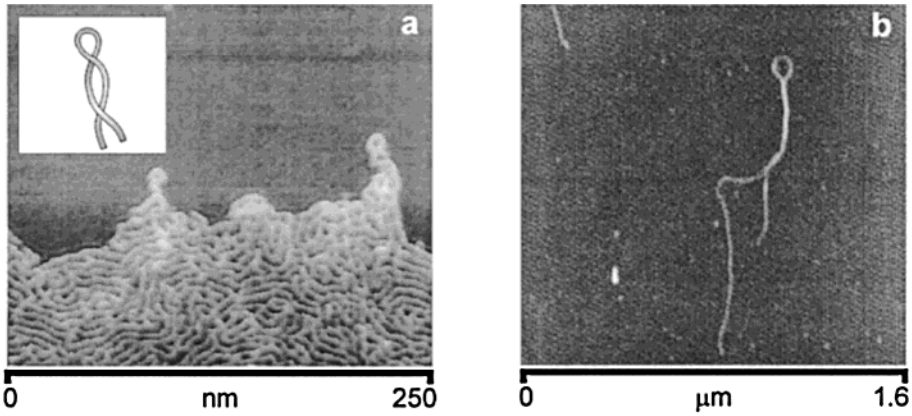

Figure 12. SFM micrographs of (a) 14-ABG-PS on mica[147] and (b) twisted ribbon structure of polypeptide β-sheets.[164] The plectoneme conformation is caused by the backward folding of the torsionally stressed molecules. Insert in a depicts a plectoneme supercoil.

by local winding up of the backbone. Regular helix formation is highly unlikely because of the atactic stereostructure and was also not observed in the mesophase state.[160] However, axial contraction must clearly be linked to local twisting. Thus, the observed supercoiling is a way of releasing torsional stress.[162,163] To the best of our knowledge, the supercoil formation of the monodendron-jacketed polystyrene is one of the first observations of a defined tertiary structure in synthetic polymers. While in biomolecules the tertiary structures are typically stabilized by specific interactions between side groups, the supercoil of the monodendron-jacketed polymers is metastable. Eventually, annealing offered a path for the stress relaxation and led to vanishing of the supercoil conformation.[147] Figure 12b shows a similar conformation observed for a polypeptide.[164]

2.4. Microscopic Structure of Adsorbed Macromolecules

How adsorption of the side chains to a flat substrate effects the backbone conformation has been observed in further microscopic detail for brush molecules with a methacrylate backbone and poly(*n*-butyl acrylate) side chains. These poly(*n*-butyl acrylate) brushes were prepared by living radical grafting from a multifunctional macromolecular initiator.[38] The synthetic approach allowed observation of the same batch of molecules without (macroinitiator) and with poly(*n*-butyl acrylate) side chains (brush).

After adsorption on mica, the SFM length of the brush molecules corresponded to an almost fully extended backbone approaching the trans zigzag conformation (Figure 13b). In contrast, the apparent length of the macroinitiator, which was scanned by SFM prior to grafting, was 2 times shorter than the contour length of the main chain (Figure 13a).

The extension of brush molecules is caused by excluded volume repulsion of the 2D-adsorbed side chains. Therefore, the length of adsorbed brushes should also depend on the grafting density. Copolymer brushes with a random sequence of methyl methacrylate and poly(*n*-butyl acrylate)-substituted methacrylate units were prepared with different compositions, i.e., grafting densities. Table 3 compares the lengths of p*n*BuA brushes with different numbers of nongrafted MMA monomers. One can see that less densely grafted brushes undergo stronger axial contraction of the main chain. When the average length of the MMA sequences became larger than four monomeric units, the observed length per monomer unit decreased significantly. This value is remarkably similar to the length $l_k \sim 12$ Å of the statistical (Kuhn) segment of PMMA.

In addition to the visualization of the molecular contour, topographic and phase contrast SFM enabled clear resolution of the fine molecular structure. Figure 14 shows SFM micrographs of single brush molecules, where one can easily distinguish both the backbone and the tightly adsorbed side chains. For example, white contours in the height micrograph (Figure 14b) correspond to the backbone wrapped by nonadsorbed side chains, while the grayish areas between the white threads demonstrate the hairy structure of the adsorbed segments of the side chains. The molecules in Figure 14a,b differ in the degree of polymerization of the side chains as $DP_n = 52 \pm 10$ and $DP_n = 10 \pm 2$, respectively. This difference was readily detected by SFM. The brushes in Figure 14a show a thicker corona of side chains around the backbone compared to the brush in Figure 14b.

The distance between the backbones in densely packed monolayers, like the one shown in Figure 14b, increases linearly with the number-average degree of polymerization of the side chains, $D \sim DP_n$. The distance is, however, significantly larger than the number-average length of a fully extended side chain, $l_0 = DP_n \times 2.5$ Å. These observations suggest that the absolute distance between adsorbed brushes is not determined by the number-average length of the side chains but it is controlled by a small fraction of longer side chains.

Extension and stiffening of the backbone because of the tight adsorption of the side chains are connected with a significant loss of entropy. A certain decrease in the entropy by bending of the backbone without changing the degree of adsorption of the side chains can, however, be enabled by an uneven distribution of the side chains between the two sides of the backbone. On the concave side of the bend, the space available per side chain is increased compared

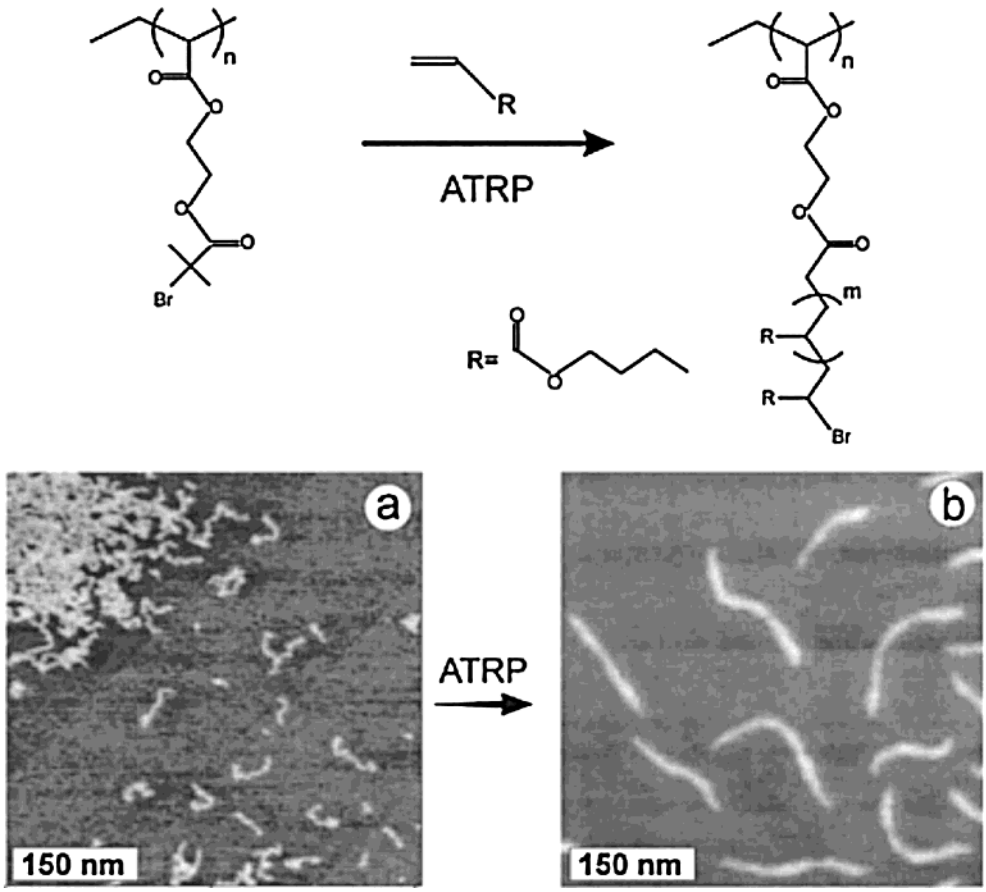

Figure 13. (Top) Preparation of PBA brushes by grafting from the macroinitiator using ATRP.[38] (Bottom) Single molecules of the macroinitiator (a) and PBA brushes (b) adsorbed on mica were visualized by tapping-mode SFM. Clearly, the grafting of long side chains led to almost full extension of the backbone approaching the contour length $L = N \cdot l_0$, where $l_0 = 0.25$ nm is the monomer length of a hydrocarbon chain in the all-trans conformation.

Table 3. Axial Contraction of p*n*BuA brushes as a Function of the Grafting Density

polymer	MMA, %	DP_n, side chains	DP_n, backbone	L_n, nm	$l_m = L_n/DP_n$, nm
homopolymer	0	35	567	123	0.22 ± 0.2
copolymer 1	35	58	477	120	0.25 ± 0.2
copolymer 2	56	42	637	127	0.2 ± 0.2
copolymer 3	77	32	710	116	0.16 ± 0.2

to the straight conformation. Thus, for these chains and the backbone, bending yields an increased configurational entropy.

Computer simulations demonstrated that such an uneven distribution of the side chains leads to bending.[165] Scaling analysis showed that the uneven side chain distribution and bending is favorable in particular for long side chains and lower grafting densities (Figure 15). In the case of an isolated single chain, bending can furthermore reduce the line tension, in the optimum case by formation of a spiral structure.[166,167]

Indeed, bending and even spiral conformations were observed for PMMA brush molecules that were deposited from a solution in THF.[165,167] This is shown by the SFM micrograph in Figure 16. Nevertheless, the situation in Figure 16 is a snapshot of a situation that emerged upon evaporation of the solvent and does not represent an equilibrium conformation.

Clear experimental evidence that the coiling of brushes on solid substrates is thermodynamically favored could be obtained in the case of the brushes with poly(*n*-butylacrylate), PBA, side chains. The low glass transition temperature of PBA ($T_g = -54$ °C) favors fast equilibration upon thermal annealing. The sample in Figure 17a was prepared by spreading a dilute solution of the PBA brush molecules in $CHCl_3$ on water (Langmuir trough). The surface pressure was increased to obtain a condensed film that was then transferred onto a mica substrate. Similar to Figure 13, the backbones were predominantly extended. This indicates a rather even distribution of the side chains to the one and the other side as it might be expected for fast adsorption at the substrate surface. When the film on mica was, however, annealed for 48 h at 120 °C, considerable coiling of the molecules occurred as shown in Figure 17b.

Summarizing the evidence from Figures 13−15 and 17, it results that the backbone conformation of the brush molecule is strongly effected by the adsorption and side distribution of the grafts. The most important contribution is the repulsion between the ad-

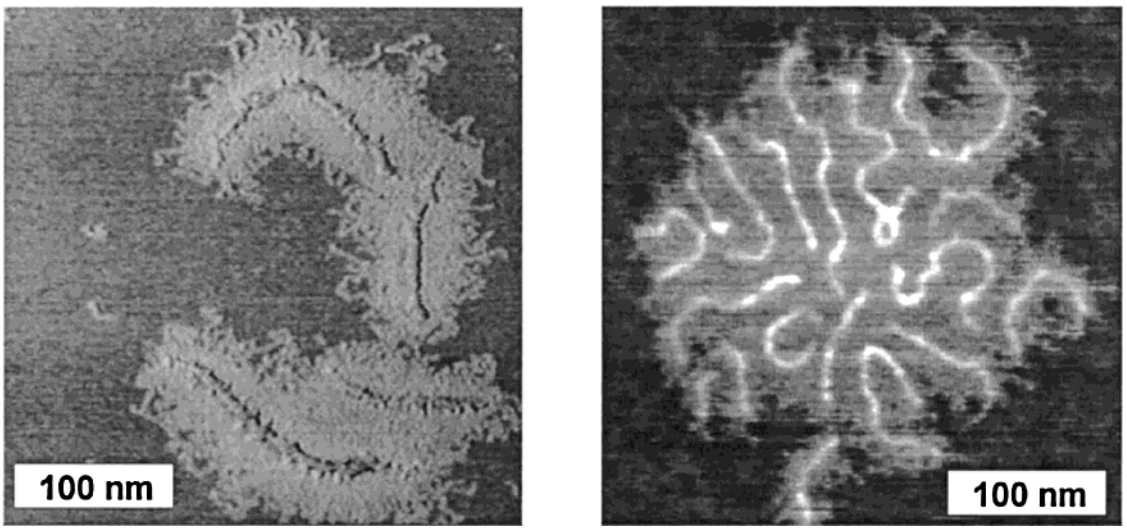

Figure 14. Molecular brushes with poly(*n*-butyl acrylate) side chains of different degrees of polymerization: (a) $n = 52$ and (b) $n = 10$.

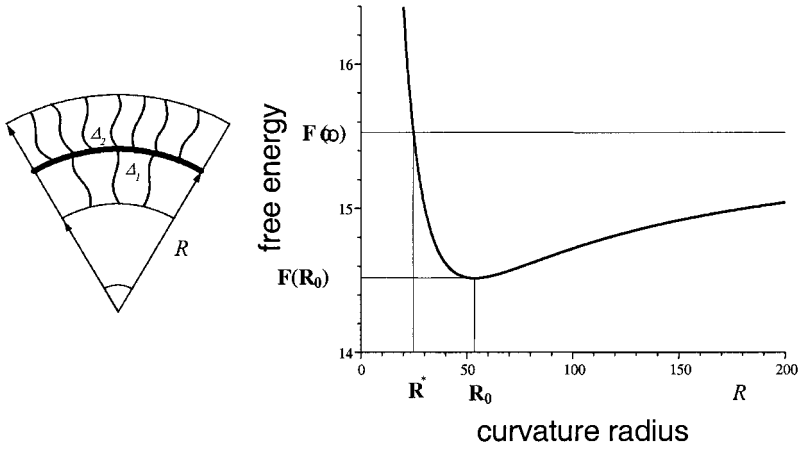

Figure 15. Calculation of the free energy of a brush molecule with asymmetrically distributed side chains as a function of the bending curvature ($DP_{side\ chains} = 100$, $\Delta_1 = 4$, $\Delta_2 = 8$, one side chain per two backbone units).

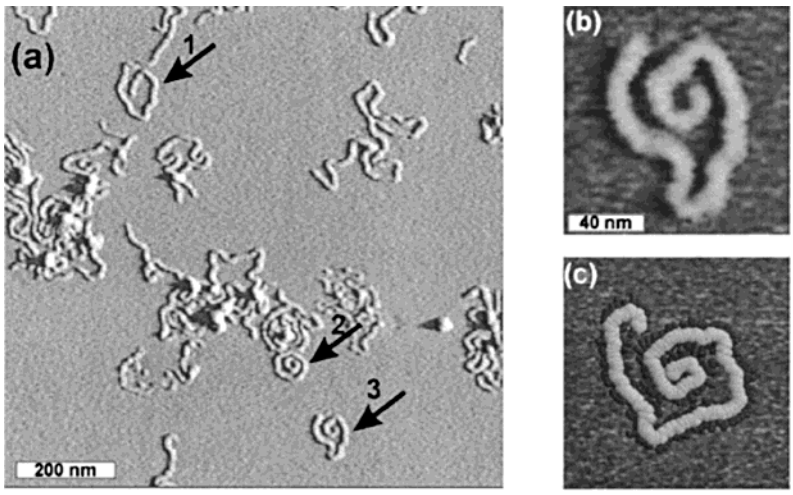

Figure 16. (a) SFM micrograph of PMMA brushes lying flat on the mica surface. The arrows show one of the typically observed conformations—2D helices of tightly winded cylindrical brushes. (b) Zoomed image of molecule 3 in part a. (c) Typical snapshot of the simulated 2*d* bottle-brush structure consisting of the 128-segment main chain and the 4-segment side chains grafted at $\sigma = 1$ and $\varphi = 0.1$.

sorbed side chains that leads to the extension of the whole brush molecule. Hence, the conformation and the persistence length must depend on the grafting density and the fractions of the adsorbed and de-

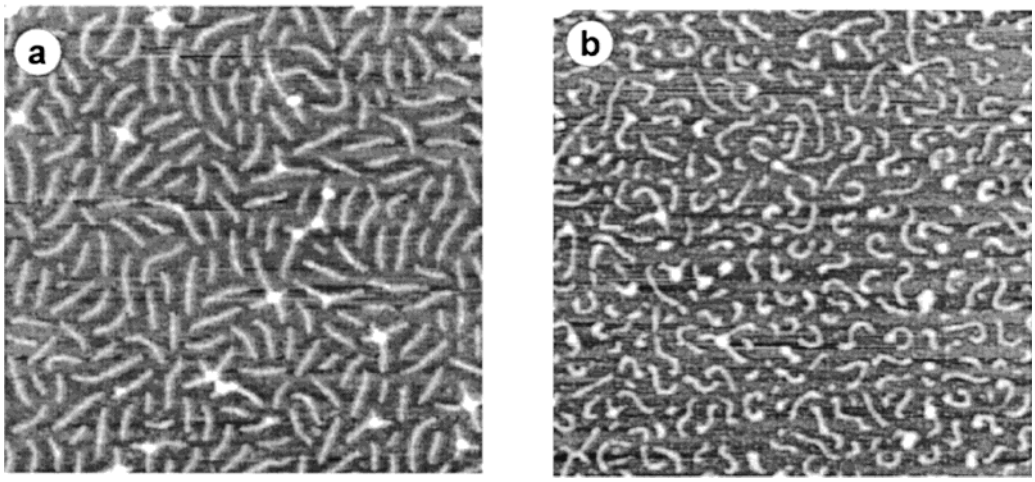

Figure 17. SF micrograph of a condensed film of poly(*n*-butylacrylate) brushes, DP $_{\text{side chain}} = 60$: (a) transferred from water onto mica and (b) after annealing at 120 °C for 48 h.

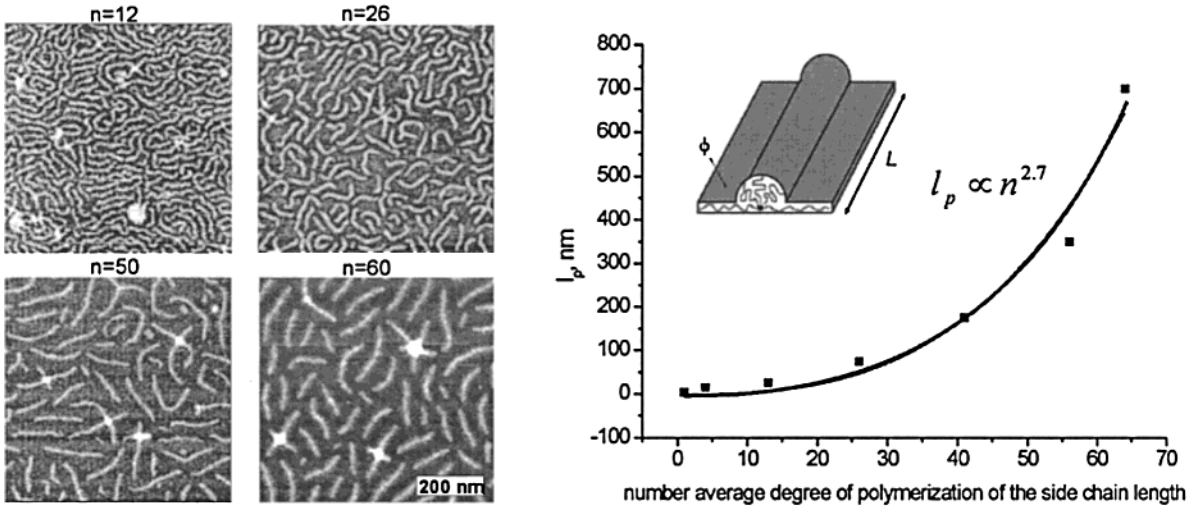

Figure 18. (Left) SFM images of poly(*n*-butylacrylate) brushes with varying degree of polymerization, *n*, of the poly(*n*-butylacrylate) side chains on mica (spin cast samples). (Right) Persistence length of a molecular brush as a function of the side chain length *n*. The continuous line describes the power function $l_p \propto n^{2.7}$ and the points experimental values from SFM.[167]

sorbed side chains. While tightly adsorbed side chains favor extension of the backbone, desorbed side chains favor the coiling process.

The dependence of the persistence length l_p on the fraction of the adsorbed side chains Θ has been derived from scaling analysis[168]

$$l_p \cong \left(\frac{\phi}{x}\right)^5 n^3 + \left(\frac{1-\phi}{x}\right)^3 n \qquad (6)$$

where $x = L/(a \cdot N)$ denotes the degree of longitudinal contraction which denotes the effective grafting density.

The degree of contraction was evaluated by minimization of the free energy of the adsorbed brush. Three contributions were considered: the elastic energy of the main and side chains, the interfacial energy, and the mixing entropy between adsorbed and desorbed chains.[168] The persistence length varies with the side chain length with a cubic power dependence $l_p \cong n^3$ in the strong adsorption regime (ϕ, $x \approx 1$) and with a square dependence $l_p \cong n^2$in the weak adsorption regime ($\phi \approx 0$, $x \cong n^{-1/3}$). The dependence of l_p on the length of the side chains can be described by a power function n^α with α varying between 2 and 3 (see Figure 18, right).

The theoretical analysis has been verified experimentally. The SFM images in Figure 18 depict the contour of four poly(*n*-butylacrylate) brushes differing in the degree of polymerization of the poly(*n*-butylacrylate) side chains. All four molecules were prepared by grafting from the same macroinitiator sample. Clearly, the extension and straightening of the molecules improved with the side chain length. The diagram in Figure 18 (right) gives a fit of the n^α dependency to experimental values. The resulting exponent $\alpha = 2.7 \pm 0.2$ is indicative of a relatively large fraction of adsorbed side chains as expected for strong interaction between the polar acrylates and the polar mica surface.

Because the adsorption of the side chains is such a strong factor in controlling the macromolecular conformation, not only the length of side chains but also their composition is of great importance. This can be demonstrated by comparing the structures for the brush molecules with poly(*n*-butylacrylate) side

Table 4. Molecular Characterization of Brush Molecules with Poly(styrene)-*block*-poly(*n*-butylacrylate) Side Chains Prepared by ATRP[169]

polymer	$M_w/10^6$ [a]	M_w/M_n	DP_{backb} [b]	DP_{core}/DP_{shell} [c]	l_m [d]
pBPEM	0.14	1.16	514		
pBPEM-*g*-p*n*BuA	1.18	1.22	514	15	0.22 ± 0.01
pBPEM-*g*-(p*n*BuA-*b*-pS)	1.85	1.24	514	15/9	0.20 ± 0.01
pBPEM-*g*-(pS-*b*-p*n*BuA)	2.49	1.26	514	27/9	0.16

[a] THF, MALLS-detector. [b] Degree of polymerization of the backbone. [c] Degree of polymerization of the side chain blocks. [d] Monomer length was calculated as $l_m = L_n/DP_n$, where $DP_n = 514$ is the number-average degree of polymerization of the main chain.

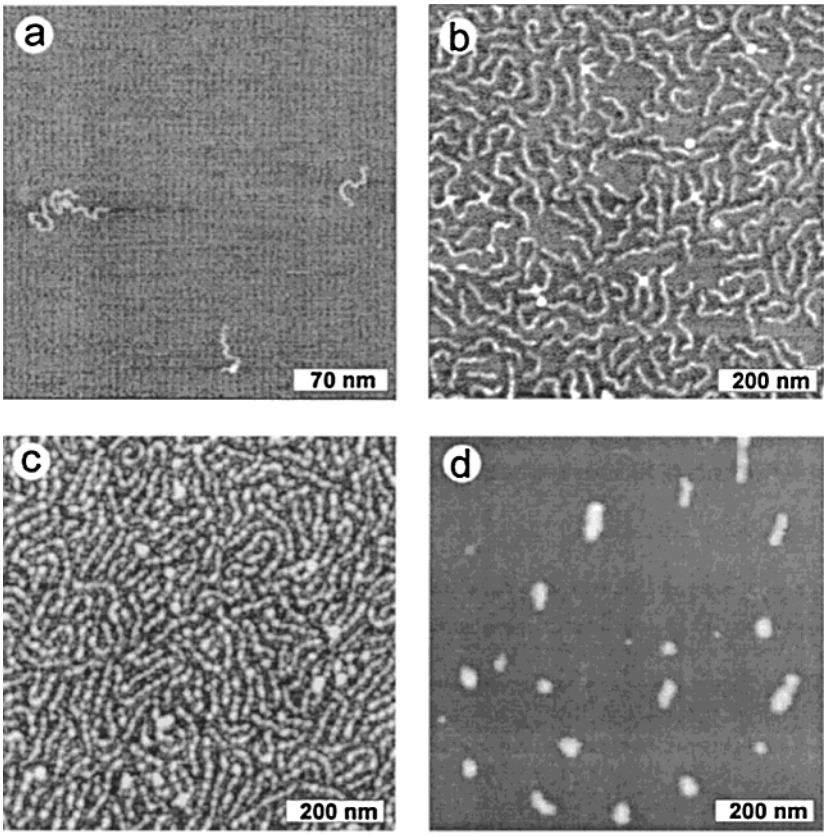

Figure 19. AFM micrographs of four different polymers adsorbed on mica: (a) single molecules of macroinitiator pBPEM, (b) monolayer of homopolymer pBPEM-*graft*-p*n*BuA brush, (c) monolayer of pBPEM-*graft*-(p*n*BuA-*block*-pS) brush, and (d) single molecules of pBPEM-*graft*-(pS-*block*-p*n*BuA) brush.[169]

chains and poly(styrene)-*block*-poly(*n*-butylacrylate) side chains, respectively. While the *n*-butylacrylate units interact strongly with a polar substrate like mica, there is a much weaker adsorption of the styrene units and correspondingly of a polystyrene brush.[169] Diblock side chains offer the possibility to distinguish between adsorption effects of the inner polymer segment, adjacent to the backbone, and the outer side chain tail.

Brushes with diblock side chains have been prepared by the same concept as illustrated in Figure 13. In this case either a polystyrene block or a poly(*n*-butylacrylate) block was grafted first by atom transfer polymerization, ATRP, on a poly(2-bromopropanoyl ethyl methacrylate), pBPEM, on which in a second step the other monomer was polymerized as the second block.[169] Table 4 summarizes the molecular structure of the corresponding polymers, i.e., (i) the macroinitiator or mere backbone molecule (pPBEM) from which (ii) a brush with p*n*BuA homopolymer side chains (pBPEM-g−p*n*BuA), (iii) a brush with an inner p*n*BuA and an outer polystyrene block (pBPEM-*g*-(p*n*BuA-*b*-PS)), and (iv) the inverse structure with an inner polystyrene and an outer p*n*BuA block (pBPEM-*g*-(pS-*b*-p*n*BuA)) have been prepared. Because all molecules have been prepared from the same macroinitiator, they have the same length, $DP_{backbone} = 514$. Due to the consequential addition of the blocks, the side chains vary in length.

Figure 19 shows SFM images of the four polymers that have been deposited by spin casting from THF solution on freshly cleaved mica. In each case, single molecules are resolved lying flat on the substrate. One clearly recognizes distinct differences in the 2D conformation, which can be attributed to the different adsorption behavior of the side chains. The images allowed one to measure the length of the macromolecules and to evaluate the contraction of the backbone relative to the contour length of the fully extended main chain.

The length of the brush molecules per monomer unit of the backbone, l_m, was evaluated from the

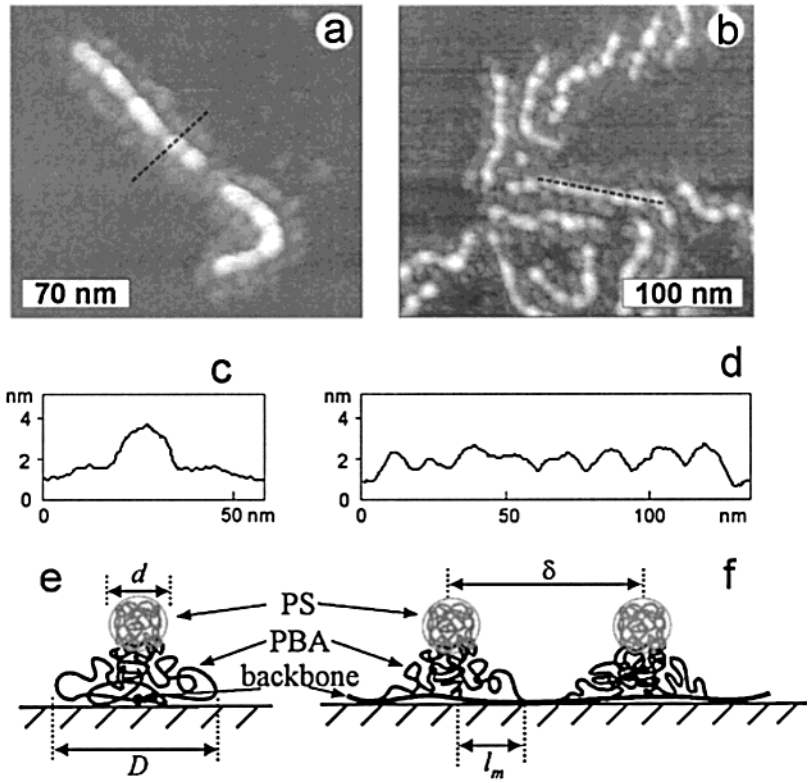

Figure 20. SFM micrographs of single molecules of pBPEM-*graft*-(p*n*BuA-*block*-pS) brushes. The cross sectional profiles (c and d) were drawn perpendicular and parallel to the molecular contour along the dotted lines in a and b, respectively. The scheme explains the necklace morphology upon looking at the molecule from the edge (e) and from the side (f).

images and compared to $l_{max} = 0.25$ nm for all-trans conformation of an aliphatic chain (Table 4). For the p*n*BuA brush, the length $l_m = 0.22$ nm indicates almost complete stretching of the backbone as shown before (Figure 14, Table 3). The p*n*BuA-*b*-pS brushes with a p*n*BuA core and a pS shell demonstrated similar extension to $l_m = 0.20$ nm. In contrast, a significantly shorter monomer length $l_m = 0.16$ nm, was determined for the inverted structure, i.e., pS-*b*-p*n*BuA with a pS core and a p*n*BuA shell. The axial contraction is consistent with the more globular conformation of the coiled up molecule morphology of the brush molecules in Figure 19d compared to those in Figure 19b,c. As might be expected, the stretching and straightening of the brush molecules are predominantly controlled by the adsorption of the side chain segments near the backbone.

The extended block-copolymer brush in Figure 19c exhibited well defined periodic undulations in thickness. This is seen in further detail in the enlarged images in Figure 20a,b. A thin corona of the tightly adsorbed chain segments is depicted surrounding the undulated backbone of the single molecule of p*n*BuA-*b*-pS in Figure 20a. The cross-sectional profiles in Figure 20d,c were recorded along the molecular backbone and perpendicular to it, respectively. After correction for the radius ($R \sim 8$ nm), the diameter of the globuli forming the necklace-like string and their separation was determined from the image to be $d = 5 \pm 1$ nm and $\delta = 15 \pm 2$ nm, respectively.

A tentative interpretation of the undulations is presented in Figure 20e,f: In contrast to the pnBA chains that adsorb flatly, the pS tails in the block-copolymer brushes tend to aggregate to clusters. The driving force might be found in entropically favorable coiling and in reduced unfavorable contacts between the pS and p*n*BuA blocks as well as between pS and air. While the PS segments form clusters, the p*n*BuA chain fragments remain tightly adsorbed on the substrate. This interpretation is consistent with the intermolecular distances *D* measured in Figure 20b,c.

3. Manipulated Conformational Transitions of Adsorbed Macromolecules

Conformational transitions and the corresponding stimuli response of macromolecules provide fundamental means for the molecular assembly and function of biological systems.[1−7] Establishing a likewise control factor in the field of synthetic macromolecules is recognized as a major challenge in nanotechnology.

According to theoretical considerations, the transition between the state of an expanded coil and a compact globule can be discrete, depending on the nature of the interaction and the chain flexibility.[170] Equilibrium coexistence of two conformations of single macromolecules as an unambiguous criterion for a first-order transition[171−174] has been clearly observed only in the case of relatively large DNA molecules.[174] However, the peculiar branching topology in dendrimers, block-copolymer micelles, and cylindrical brushes provides a unique means to introduce the competitive interactions necessary for a conformational transition.[168,175−177] In the following it will be shown that coexistence between an extended and a globular conformation can occur in the case of poly(*n*-butyl acrylate) brush molecules[168] and be visualized in detailed resolution on a significantly smaller length scale than possible in the case of DNA.

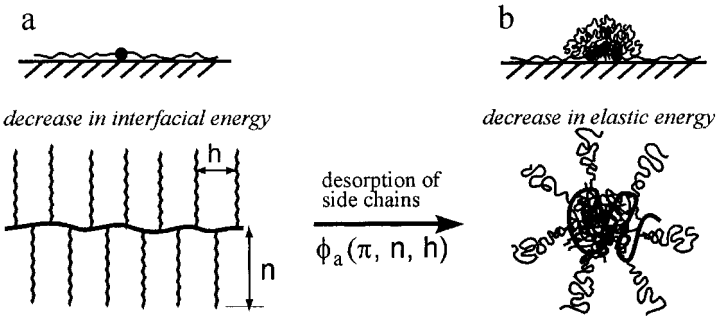

Figure 21. Conformations of cylindrical brushes upon adsorption on a surface: (a) extended chain, (b) globule.

Table 5. Molecular Characterization of the PBPEM Macroinitiators and the Corresponding PBA Brushes by Multiangle Laser Light Scattering Size Exclusion Chromatography (MALLS−SEC) and Static Light Scattering (SLS)[168]

	macroinitiator			brush		
polymer	M_w,[a] g/mol	M_w/M_n	N^b	M_w,[c] g/mol	M_w/M_n[d]	n_{LS}[e]
A	2.2×10^5	1.3	641	4.6×10^6	1.1	46
B	1.6×10^5	1.3	453	1.6×10^6	1.2	20
C	1.8×10^5	1.4	490	1.4×10^6	1.3	15

[a] By MALLS−SEC using dn/dc=0.084 (error bar 5%). [b] Number-average degree of polymerization calculated as $N = M_n/M_0$, where $M_0 = 265$ g/mol − molecular weight of the monomer unit of pBPEM. [c] By SLS using the refractive-index increment dn/dc = 0.068. [d] Polydispersity from MALLS−SEC. [e] The number-average degree of polymerization of the side chains was determined as $n_{LS}=(M_n - M_0)/m$, where m = 128 g/mol − molecular weight of BA and M_n = number-average molecular weight of the PBA brush measured by MALLS-SEC and SLS.

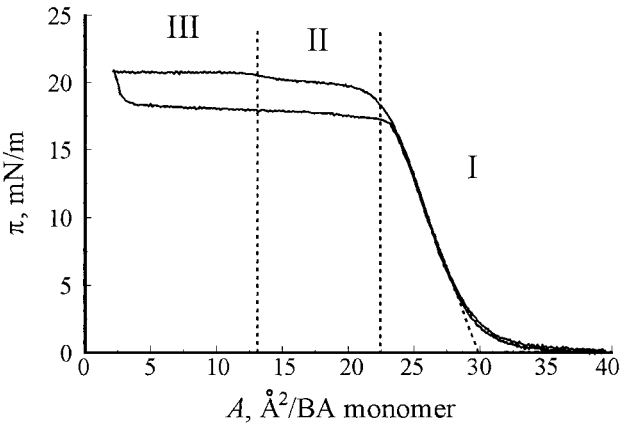

Figure 22. Langmuir isotherm for the compression of a monolayer of poly(*n*-butyl acrylate) brush molecules with the degree of polymerization of the side chains $n = 46$.[168]

As discussed above, the conformation of molecular brushes at an interface is determined by the interaction of the side chains with the substrate and entropic flexibility of both the side chain and the flexible backbone. The stretched backbone conformation of pnBA brushes depicted in Figures 13, 14, 17, and 18 is enabled by a large number of energetically favorable surface contacts. One can envision a transition to a globular conformation if the interaction strength is reduced and coiling becomes entropically favored at the expense of the surface contacts. Since the energy and the entropy contribution vary differently with respect to contact area and interaction strength, the brushes can undergo a transition at a critical interaction strength at which the free energies of the stretched and collapsed state become equal. Such a transition may occur upon changing thermodynamic variables, e.g. solvent quality and temperature, or under the effect of an external field. Thus, instead of variation of the interfacial energies, the number of surface contacts available per molecule or side chain can be altered by reducing or expanding the surface area per molecule as done experimentally on a Langmuir trough. In this case the free energies of the extended and collapsed state become equal at a critical surface pressure, at which point the brushes can undergo a transition. The concept is schematically depicted in Figure 21 and has been realized in experiment with pnBA brush molecules.[168]

Table 5 lists the molecular structure parameters of three different pnBA brush molecules basically differing in the length of the side chains, which were determined by size exclusion chromatography and light scattering in dilute solution.

Owing to the amphiphilic nature of *n*-butyl acrylate groups, the pnBA brushes spread on a water surface. Figure 22 shows a $\pi-A$ isotherm (surface pressure versus monolayer area per BA residue) for polymer A with the longest side chains. Corresponding to the low glass transition temperature, $T_g = -54$ °C, compression of the PBA brushes was fully reversible as expected for equilibrium spreading. The pressure onset occurred at about 35 Å^2 and rose until a critical area of 22 Å^2, at which the pressure leveled off at 19.5 mN/m. The plateau between 22 and 13 Å^2 was followed by a second plateau with a distinct increase in pressure from 19.5 to 21 mN/m. The linear extrapolation of the isotherm to zero pressure gave the area $a_0 = 28 \pm 1$ Å^2, which is consistent with the monomer area of 29.3 Å^2 measured for linear PBA. The values indicate that practically all BA monomer units are in contact with the water surface, whereby the butyl tails are oriented toward air perpendicular to the surface. The plateau between 22 and 13 Å^2 is remarkable and indicates a structural transition within the monofilm.

The molecular structures at the different stages of compression were visualized by SFM on samples that were transferred onto a mica substrate while the pressure was kept constant. Figure 23 shows such a series of SFM micrographs obtained at different compression.

In each micrograph, the brush molecules were clearly resolved individually. At areas above 22 Å^2

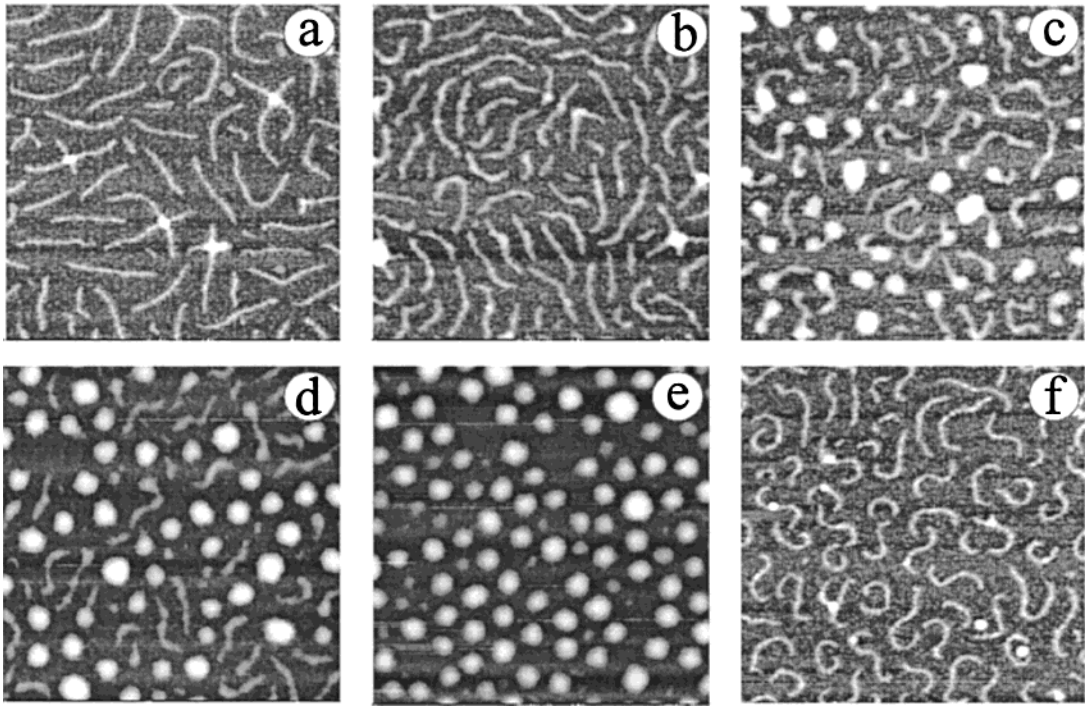

Figure 23. SFM micrographs of monolayers of pnBA brushes (sample A in Table 5) transferred on mica at different degrees of compression: (a) 30 Å^2, (b) 23 Å^2, (c) 21 Å^2, (d) 17 Å^2, (e) 13 Å^2, (f) 30 Å^2 (after expansion).[168]

the molecular cylinders retained their stretched conformation but became packed increasingly dense. The wormlike entities in Figure 23a, b mark the contour of the backbone and represent the extended brush molecules as depicted in Figure 21a. The space between is occupied by the fraction of the side chains which are tightly adsorbed. The fundamental collapse of the wormlike structure predicted above was observed in the transition zone between 22 and 13 Å^2. The SFM images in Figure 23c−e demonstrate that the molecules became more flexible and coiled, while at the same time a significant decrease in length is observed. The round spots in Figure 23c−e are assigned to single molecules which collapsed to a pancake-like or nearly globular structure as illustrated in Figure 21b. As the number of chains in Figure 23a and number of globuli in Figure 23e was fairly equal, it was concluded that the molecular collapse is accompanied by desorption of the side chains from the water surface and is occurring in first as an intramolecular collapse and only in a later stage by intermolecular aggregation as the collapsed molecules get piled up.

The observed conformational transition was analyzed theoretically assuming partial desorption of the side chains under compression, i.e., upon variation of the spreading parameter.[168] The total free energy $F = F_{el}^{2D} + F_{el}^{3D} + F_s + F_{mix}$ (F_{el} = elastic contribution to the free energy, F_s = surface energy of the brush, F_{mix} = mixing entropy of the side chains) was minimized with respect to two independent variables: the fraction of adsorbed 2D chains, ϕ_a, and the relative contour length of the brush, L/aN. Above a critical length of the side chains, the free energy has two minima, i.e., (i) the extended brush with a large fraction of adsorbed side chains and (ii) the collapsed globuli with a smaller fraction of adsorbed side chains. Since the free energies of these two conformations depend in an opposite way on the interaction strength, the variation of either the area available per molecule A or the spreading parameter $S = \gamma_1 - \gamma_{12} - \gamma_2$ can cause a discontinuous first-order transition from one state to the other. The results of the evaluation are summarized in Figure 24, where the fraction of adsorbed side chain units is plotted against the surface pressure and the critical surface pressure S_c is plotted against the inverse length of the side chains $1/n$.

Switching between two distinct conformations has been observed also for spherical branched particles such as block copolymer micelles. Block copolymers of poly(styrene) and poly(*N*-alkyl-4-vinylpyridinium iodide) were aggregated to micelles with a polystyrene core and a poly(*N*-alkylpyridinium iodide) corona. These micelles could be spread on water from a solution in $CHCl_3$ and compressed to a monofilm[170] (Figure 25b). Due to the amphiphilicity of the *N*-alkylpyridinium iodides, the poly(pyridinium iodide) block gets adsorbed in a 2D conformation with the *n*-alkyl groups pointing to the air. Upon lateral compression of the condensed monofilm of surface micelles, also in this case, a distinct phase transition was observed upon lateral compression as the corona chains got desorbed from the water/air interface (Figure 25a). The transition was particularly pronounced in the case of longer chains, i.e., *n*-octyl pyridinium groups. The cooperative desorption/collapse is consistent with recent X-ray reflectivity data.[178]

4. Motility of Molecules

So far we have encountered two particular features of the conformation of brush molecules adsorbed on

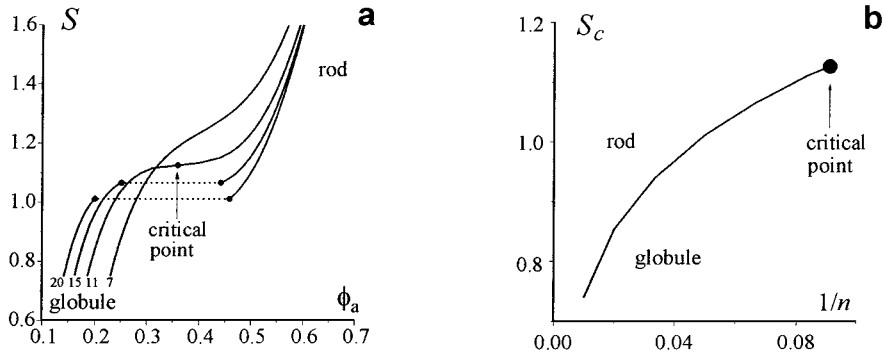

Figure 24. Phase transition from the extended coil to a globule state as found by scaling analysis. The transition is caused by lowering the surface pressure below a certain critical value S_c at which the fraction of adsorbed monomers $\phi_a = N_{2D}/N$ undergoes discrete changes (a). Hereby, the S_c depends critically on the side chain length (b).[168]

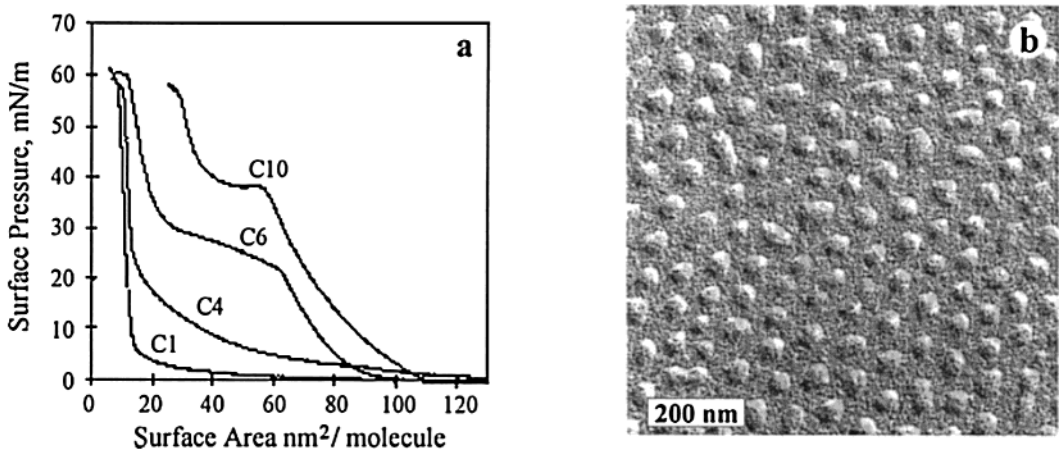

Figure 25. Surface pressure−area/molecule isotherms of Langmuir films (a) of $(PS)_{260}(RPVP^+I^-)_{240}$, where the P4VP block was quaternized with different *n*-alkyliodides R = C_1, C_4, C_6, C_{10}. Metal-shadowed TEM micrographs (b) of the LB films of $P(S_{260}$-*b*-VP_{71}/C10I) deposited on a carbon-coated surface at 2 mN/m from a pure water surface.[178]

a flat surface. These are (i) the observation that the brush gets stretched as the side chains get confined to a 2D layer upon adsorption and (ii) the observation that the 2D brush winds up if the side chains get distributed unevenly between the two faces of the backbone. Both effects provide an intriguing access to stimulated molecular action. For example, if we assume a tightly adsorbed brush molecule with two different side chains whose mutual interaction parameter can be switched from attractive to repulsive by an external field, such a molecule can undergo a stimulated transition from an extended (even distribution of side chains) to a curled conformation (uneven distribution of the side chains). Yet, we cannot propose a realistic concept for such a system. However, a molecular rod−coil actuator appears to be much more feasible based on the experiments summarized in Figures 21−25. Besides the variation of the surface pressure used in the experiment in Figure 22, stimulated adsorption/desorption of a brush molecule can, in principle, be achieved by a number of means, e.g., photoisomerization of suitable groups in the side chains, by mechanical interaction with the tip of a scanning probe microscope, or by changes of the temperature. The latter means have the advantage that isolated molecules can be addressed also in contrast to the isothermal compression of a monofilm.

Ultimately, a stimulated molecular action like the stretch−coiling transition can form a basis for molecular motility and the development of molecular motors. Complex protein molecules such as kinesin, myosin, and dynein are examples of molecular motors from biology. These molecules can undergo directed movement along cytoskeletal filaments based on coordinated conformational changes which lead to periodic adsorption and detachment of molecular fragments on the filament surface.[179−183] The movement occurs via a sequence of elementary steps which are driven by ATP hydrolysis,[184] but the steps can take place stochastically and some of them are directed backward.[185] Respectively, two models have been proposed to explain the motion of motor proteins: single-step directed motion and the biased Brownian ratchet model.[184,185] In the latter case an anisotropic ratchet potential is turned off and on. This way the Brownian motion of a particle can be transformed into a directed motion.[186]

In the following we want to discuss, first, experiments on the motility of brush molecules based on stimulated desorption/adsorption. The stimulation is effected by the tip of a scanning force microscope as the molecules are probed. Essential questions are whether this can cause mobility different from Brownian motion but also different from dragging of the molecules. For comparison, we summarize results on the dragged motion of a λ-phage DNA through an entangled solution and the Brownian motion of DNA molecules adsorbed on a fluid lipid membrane.

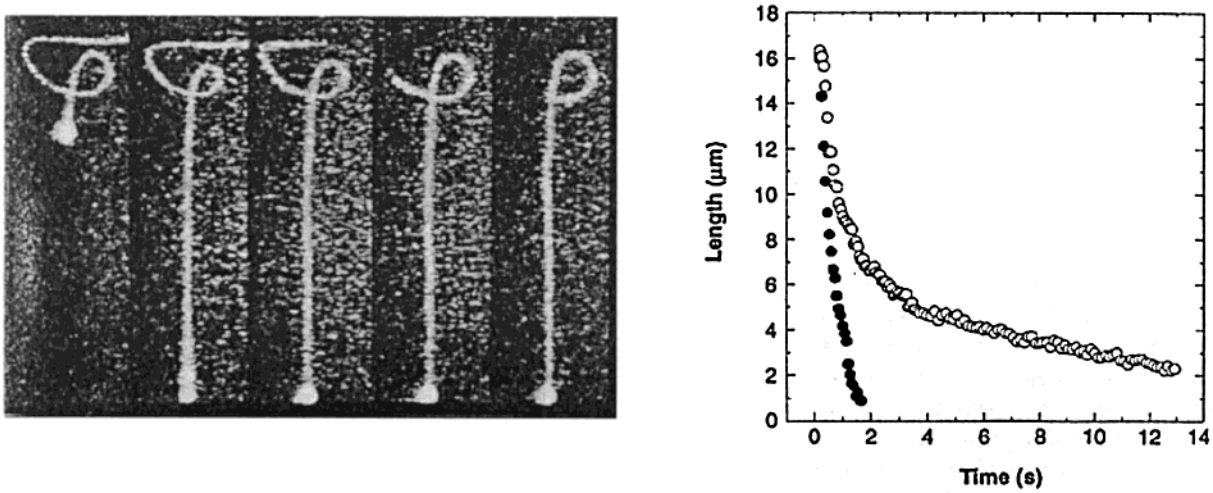

Figure 26. (a) Tiled series of images showing tube deformation and stress recovery in a concentrated polymer solution. The times for images are 0, 0.3, 1.6, 2.3, 3.0 s. (b) Comparison of the relaxation of a 17 mm molecule linearly stretched to full extension at 80 mm/s in (○) concentrated polymer solution and in (●) pure solvent.[65]

4.1. Dragged Motion of λ-DNA

Recent developments of optical trapping and fluorescent labeling techniques allowed detection and probing of single molecules.[65,142] To test the dragged motion and relaxation of a single macromolecule, the end of a fluorescently labeled λ-phage DNA was chemically linked to a latex bead and dragged by means of optical tweezers through an entangled solution of nonlabeled molecules at velocities from 5 to 100 μm/s. As the test chain was pulled or relaxed through the concentrated polymer solution, it closely followed the path of the bead (Figure 26a). The motion through the entanglement network was shown to be much different from the motion in a viscous Newtonian fluid, where the chain moved in a direction perpendicular to its contour. As the bead was rapidly moved away from the loop, tension in the chain increased and the loop was pulled tight. When the bead stopped, the loop recovered to the original size.

4.2. Brownian Motion of Adsorbed λ-Phage DNA

As discussed before for the example in Figure 5, DNA chains are confined to two dimensions but are free to diffuse laterally if they get adsorbed to a fluid lipid membrane. The microscopy experiments of the fluorescence-labeled molecules also allowed direct analysis of the chain dynamics, self-diffusion of the molecules, and conformational relaxation as a function of the chain length.[140] With the exception of a number of molecules that showed anomalous diffusion attributed to surface defects, the overall motion was described by the mean-square displacement linear in time: $\langle |R_{cm}(t) - R_{cm}(0)|^2 \rangle = 4Dt$. The diffusion coefficient D_{cm} (center of mass) decreases inversely proportional to the length of the polymer as predicted for the dynamical scaling of the Rouse model, $D_{Rouse} \sim N^{-1}$, in the absence of hydrodynamic interaction.[187,188] Fitting of the experimental data yielded $D_{cm} \sim N^{0.95\pm0.06}$ (Figure 27b). Hence, the 2D diffusion is substantially different from DNA three-dimensional self-diffusion in bulk, where long-ranged hydrodynamic interaction plays a dominant role.[142,189]

One can also analyze the rotational relaxation of the adsorbed molecules.[140] Figure 27a shows a time sequence of a single molecule with an overlay of the unit vector $u(t)$ defined as the direction of the longer principal axis of the gyration tensor. An instantaneous polymer configuration may be described by an ellipse, and therefore, the simplest conformational change is the rotational motion of an ellipse. The time correlation function of $u(t)$ decays exponentially where τ_r denotes the rotational relaxation time, $\langle u(t)u(0) \rangle \propto \exp(-t/\tau_r)$.

As shown in Figure 27c, the rotational relaxation time varies as a power of length, $\tau_r \propto N^{\mu}$ with $\mu = 2.6 \pm 0.4$. The experimental result is in remarkable agreement with the scaling behavior of the rotational relaxation $\tau_r \propto N^{1+2\nu}$ with $\mu_{theory} = 2.5$, which follows from the Rouse model and the Flory exponent $\nu = 3/4$.[189]

4.3. Stimulated Motion of Monodendron-Jacketed Polymers

The observation that a macromolecular brush gets stretched as the side chains get adsorbed on a flat surface provides a means to stimulate molecular motility by desorption of the brush molecule or a segment of it. If the molecule is in a subsequent period allowed to relax to the adsorbed stretched state it will eventually do a step forward. This is depicted schematically in Figure 28 as a sort of a creep motion. Here, the desorbed state might be characterized as an excited state whose formation requires input of energy. In the case that the structure of the surface and of the molecule favor relaxation into a distinct direction, i.e., in the case of an asymmetric potential, the motion of the molecule can be become directed.

The examples shown in Figures 7, 8, and 11 of the monodendron-jacketed polymers adsorbed on HOPG demonstrated that these macromolecules orient along the main axes of graphite. Thus, relaxation by adsorption according to the scheme in Figure 28 will be directed along these axes, either forward or backward. In particular, if the desorption effects only

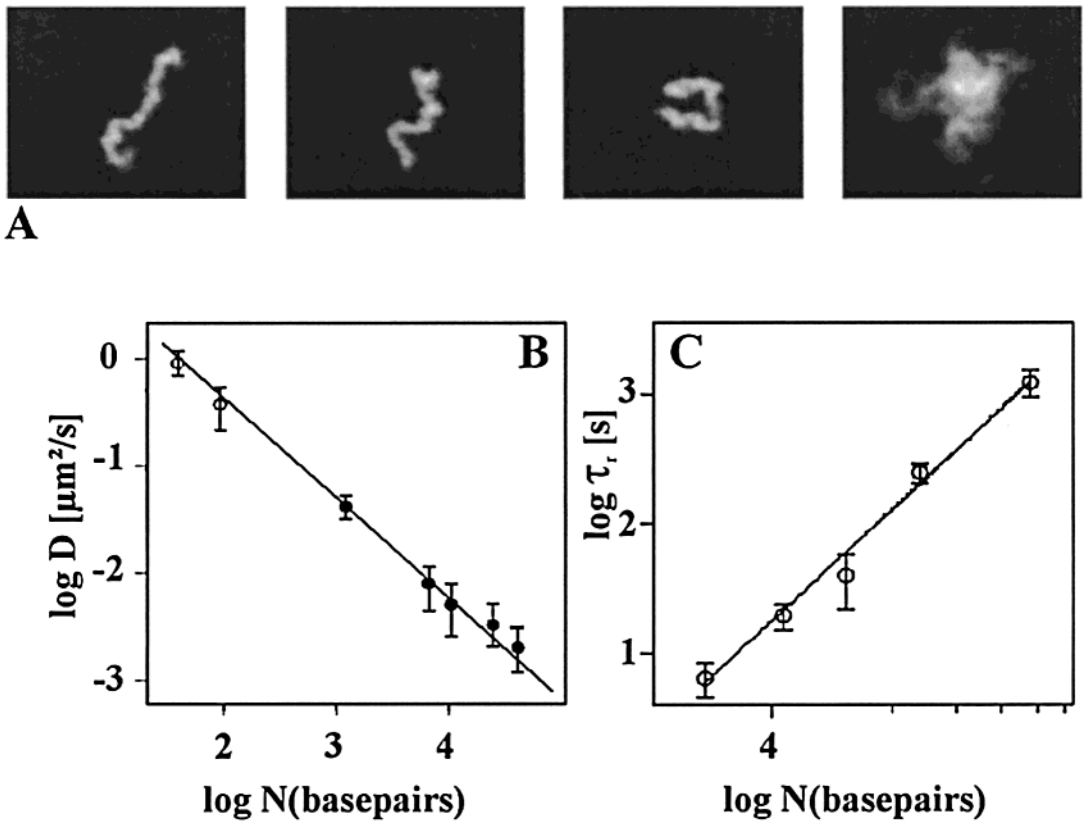

Figure 27. Dynamical scaling of DNA confined to the surface of a supported lipid membrane. (a) Time sequence ($\Delta t = 30$ s) of a DNA molecule diffusing on a cationic lipid membrane. The image on the right depicts an overlay of 16 images: time average yields a smeared fluorescence distribution. (b) Scaling behavior of the self-diffusion coefficient of the center of mass D with the number of base pairs. (c) Scaling behavior of the rotational relaxation time τ_r with the number of base pairs.[140]

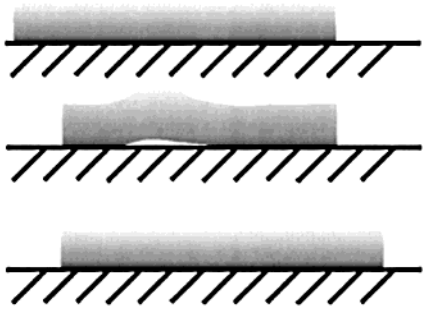

Figure 28. Creep motion by contraction upon desorption and subsequent stretching upon adsorption of an abstract molecular object.

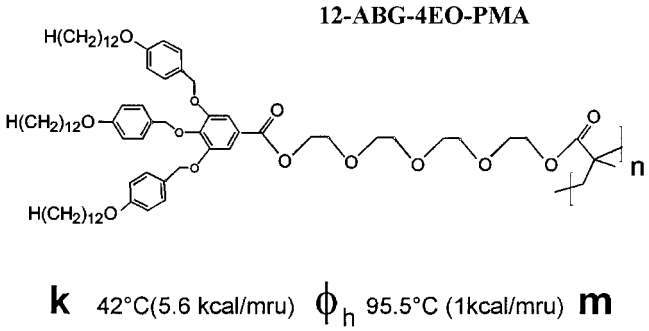

Figure 29. Chemical structure and phase transitions of 12-ABG-4EO-PMA.

a segment of the molecule as depicted in Figure 28, it will keep some memory of its original orientation toward the substrate and eventually follow this line. The examples of the pnBA brushes in Figures 14 and 23 have demonstrated that the transition between the stretched and the coiled conformation is particularly pronounced for comb or brush molecules with long side chains that adsorb tightly. Combination of both structural features might, thus, be expected to allow a creeping step in a preferred direction.

Figure 29 depicts the molecular structure of a polymethacrylate where each monomer unit has been substituted by a tris(*p*-undecyloxybenzyloxo)benzoate unit via a tetraethylenglycol spacer. From the molecules, which we have been able to study so far, this is the structure that suits the model best. For the bulk structure a transition from a low-temperature crystal phase to a hexagonal columnar state ϕ_h has been found at 42 °C. Axial extension by ca. 7% has been found by X-ray upon transition from the crystalline to the hexagonal phase.[160]

Similar to the other monodendron-jacketed polymers discussed above, also 12-ABG-4EO−PMA orders along the main axes of HOPG upon adsorption. Figure 30 shows on the right side a scanning force micrograph with a number of single molecules that have been deposited from dilute solution on HOPG.

A scanning force microscope equipped with a temperature cell enabled in-situ monitoring of the motion of the single molecules and small molecular clusters at elevated temperature.[190] The diagram on the left side of Figure 30 depicts the traces of the molecules that were recorded by imaging the sample within intervals of 4 h 20 min over a period of 12 h at 35

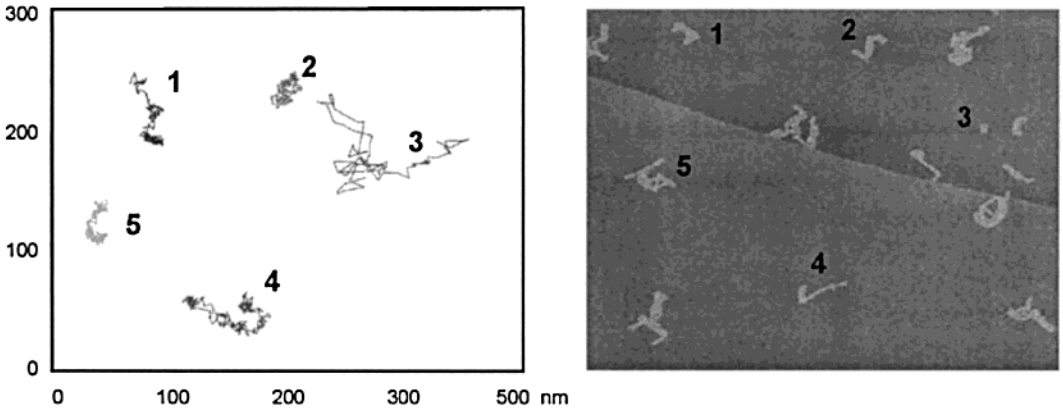

Figure 30. Random walk of single molecules as observed in situ by tapping-mode SFM at 35 °C.

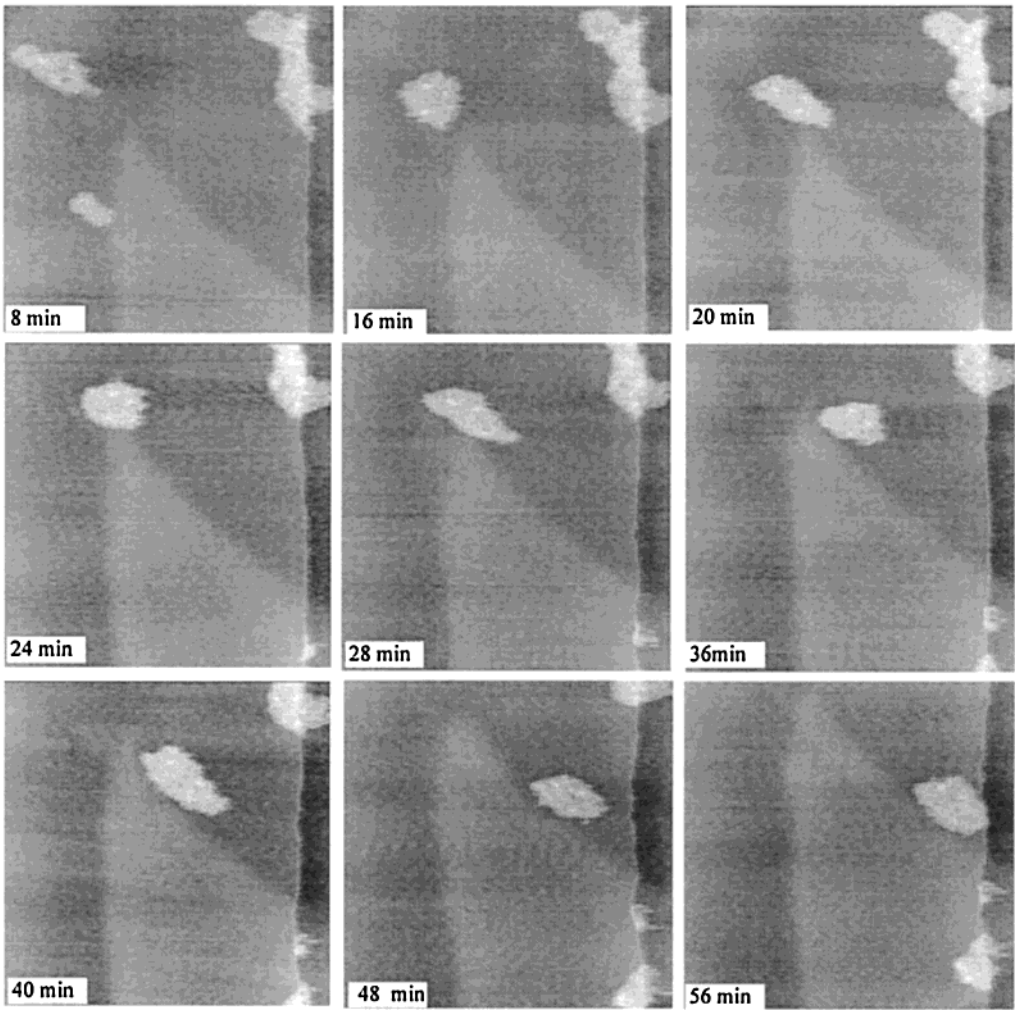

Figure 31. Persistent motion of a small cluster of five 14ABG-4EO−PMA molecules along the terrace of HOPG at 40 °C. The width of each image corresponds to 486 nm.

°C. The motion patterns are consistent with a random walk, i.e., a mean square displacement linear in time, $\langle \Delta R^2 \rangle = 4Dt$. Evaluation of the time dependencies yielded diffusion coefficients for each molecule, e.g., for the five molecules/clusters marked by the numbers in Figure 30, the following diffusion coefficients were obtained: $D(1) = 0.01$ nm^2/s; $D(2) = 0.09$ nm^2/s; $D(3) = 1.7$ nm^2/s; $D(4) = 0.04$ nm^2/s; $D(5) = 0.06$ nm^2/s. Within the accuracy of the evaluation procedure (± 0.02 nm^2/s) the following trends could be deduced from the observation of more than 100 molecules: (i) The diffusion becomes faster upon raising the temperature; (ii) smaller molecules or clusters of a few molecules exhibit a higher mobility then larger ones, (iii) within certain time intervals the molecules appear to be tight to yet unknown obstacles on the substrate, so that they can only sway around, (iv) some molecules move along a distinct line that is probably a defect in the surface structure of HOPG, e.g., a grain boundary, (v) molecules can show an increased mobility characterized by a diffusion coefficient that is 10−20 times larger than the average

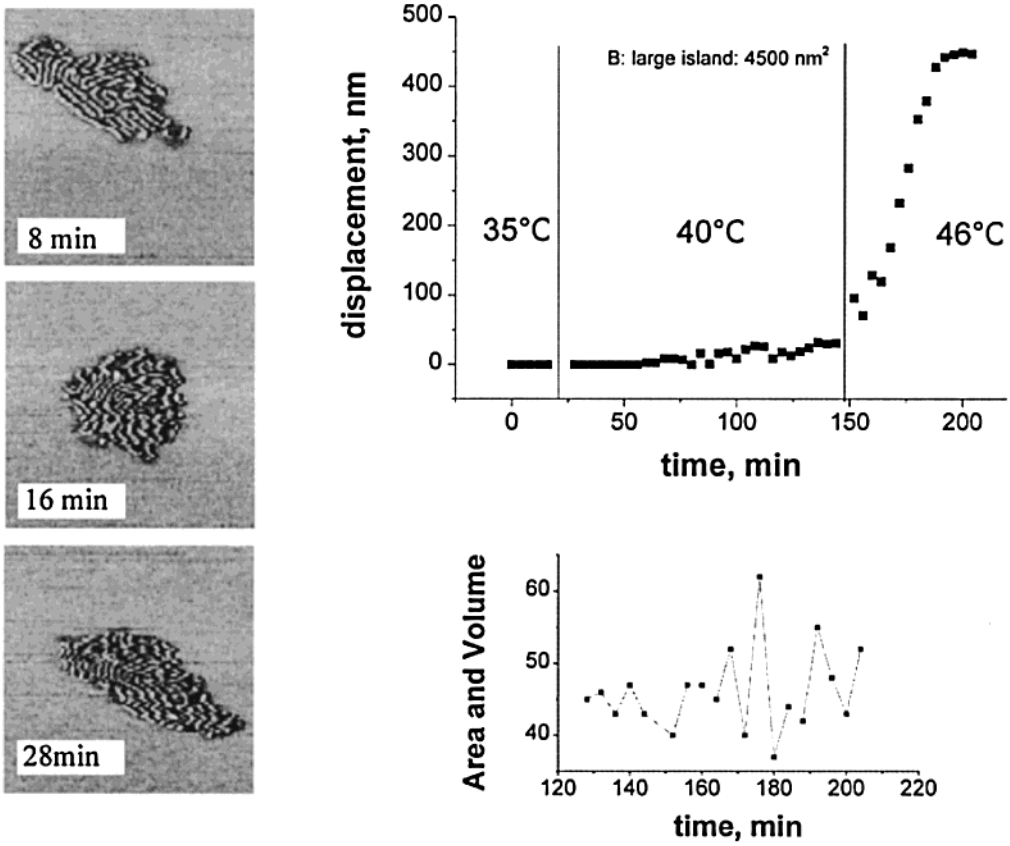

Figure 32. Time variation of (a) the displacement and (b) cluster size during its motion on HOPG at 46 °C. The in-situ-measured SFM micrographs depict momentary shape and inner structure of the cluster including packing of the molecules at different intervals after the motion started—8, 16, and 28 min.

value (see 3 in Figure 30). The two latter observations can be seen as an indication that the motion can be guided by the substrate and eventually switch for some time to a higher "gear". This, however, will require a mechanism other than Brownian motion.

That the motion can, indeed, change significantly was observed for larger clusters of a number of molecules at further elevated temperature. Figure 31 shows a series of six micrographs captured during a time period of 1 h at a temperature of 46 °C. One can clearly see that a small cluster consisting of ca. five molecules moves steadily along the terrace of the HOPG substrate. The motion started at 46 °C and continued for 60 min until the cluster got trapped in the gusset formed by two terraces on the HOPG surface.

Besides the remarkable directionality of the motion, the images demonstrate also a periodic variation of the cluster from an elongated to a circular shape. The diagrams in Figure 32 depict the time dependence of the displacement and the cluster size. Until the cluster was finally trapped, the speed remained fairly constant, as can be seen from the constant slope in Figure 32a. The oscillatory variation of the cluster area and shape is shown in the graph in Figure 32b.

The motion can be explained according to the coarse model depicted in Figure 28. Although the actual cause of the motility remains unknown, local perturbations of the molecular structure are believed to be caused by the mechanical contact with the scanning tip.[190] Clearly, the SFM images shown in Figure 32 demonstrate an alternation form a more-ordered to a less-ordered structure and vice versa. Systematic variation of the tapping parameters have demonstrated further that the well-ordered structure formed after relaxation can be disordered by the interaction with the probing tip. This occurs without direct displacement of the cluster of molecules. A quantitative and more detailed study of this phenomenon is still in progress.

5. Synopsis

The examples discussed above demonstrate that the complex architecture of hyperbranched and brush-like macromolecules can lead to properties and characteristics in the molecular conformation that are not known for linear macromolecules. Competing effects at different length scales result in very peculiar ordering and transformations. The not yet proven model of a molecular motion demonstrates how the interplay of the different interactions and elastic forces might be exploited for creating a molecular walker. While on one hand the adsorption of the molecules on a flat surface is necessary to perform SFM studies on macromolecules with molecular resolution, the surface interaction also causes, on the other hand, a perturbation that can be manipulated in very specific ways. Here we proposed that the localized interaction of the probing tip of a scanning probe microscope can be exploited to stimulate macromolecules to move according to their particular relaxation modes. Other means to apply an external field can be considered such as photo-

chemical transformations or varying electrical or magnetic fields. This way it will be possible to develop more perfected approaches to design sophisticated functional systems based on hyperbranched molecules.

6. Acknowledgment

The authors are indebted to Profs. Oleg Borisov, Alexei R. Khokhlov, Krzysztof Matyjaszewski, Aziz Muzafarov, Virgil Percec, Igor Potemkin, and Manfred Schmidt for a long-standing fruitful cooperation. We also acknowledge the experimental help of Ahmed Mourran, Svetlana Prokhorova, David Shirvaniants, and Bernd Tartsch. Financial suuport was provided by the Deutsche Forschungsgemeinschaft (SH 46/2-1; GRK-328: "Molecular organization and dynamics on surfaces and interfaces", SFB 569 "Hierarchic Structure Formation and Functions of Organic-Inorganic Nanosystems").

7. References

(1) Stayton, P. S.; Shimoboji, T.; Long, C.; Chilkoti, A.; Chen, G.; Harris, J. M.; Hoffman, A. S. *Nature* **1995**, *378*, 472.
(2) Mao, C.; Sun, W.; Shen, Z.; Seeman, N. *Nature* **1999**, *397*, 144.
(3) Montemagno, C.; Bachand, G.; Stelick, S.; Bachand, M. *Nanotechnology* **1999**, *19*, 225.
(4) Noji, H.; Yashuda, R.; Yoshida, M.; Kinosita, K., Jr. *Nature* **1997**, *386*, 299.
(5) Dennis, J. R.; Howard, J.; Vogel, V. *Nanotechnology* **1999**, *19*, 232.
(6) Lu, H.; Schulten, K. *Biophys. J.* **2000**, *79*, 51.
(7) Jelezko, F.; Tietz, C.; Gerke, U.; Bittl, R.; Wrachtrup, J. *Single Mol.* **2000**, *1*, 184.
(8) Holerca, M. N.; Percec, V. *Biomacromolecules* **2000**, *1*, 6.
(9) Stapert, H. R.; Nishiyama, N.; Jiang, D.-L.; Aida, T.; Kataoka, K. *Langmuir* **2000**, *16*, 8182.
(10) Davis, A. P. *Nature* **1999**, *401*, 120.
(11) Kelly, T. R.; de Silva, H.; Silva, R. A. *Nature* **1999**, *401*, 150.
(12) Koumura, N.; Zijlstra, R. W.; van Delden, R. A.; Harada, N.; Feringa, B. L *Nature* **1999**, *401*, 152.
(13) Collier, C. P.; Wong, E. W.; Belohradský, M.; Raymo, F. M.; Stoddart, J. F.; Kuekes, P. J.; Williams, R. S.; Heath, J. R. *Science* **1999**, *285*, 391.
(14) Kwon, I. C.; Bae, Y. H.; Kim, S. W. *Nature* **1991**, *354*, 291.
(15) Antonietti, M.; Basten, R.; Lohmann, S. *Macromol. Chem. Phys.* **1995**, *196*, 441.
(16) Baumann, F.; Deubzer, B.; Geck, M.; Dauth, J.; Sheiko, S. S.; Schmidt, M. *Adv. Mater.* **1997**, *9*, 955.
(17) Senff, H.; Richtering, W.; Norhausen, Ch.; Weiss, A.; Ballauff, M. *Langmuir* **1999**, *15*, 102.
(18) Dvornic, P. R.; Tomalia, D. A. *Curr. Opin. Colloid Interface Sci.* **1996**, *1*, 221.
(19) Fréchet, J. M. J.; Henmi, M.; Gitzov, I.; Aoshima, S.; Leduc, M. R.; Grubbs, R. B. *Science* **1995**, *269*, 1080.
(20) Newkome, G. R.; He, E.; Moorefield, C. N. *Chem. Rev.* **1999**, *99*, 1689.
(21) Fischer, M.; Vögtle, F. *Angew. Chem., Int. Ed. Engl.* **1999**, *38*, 884.
(22) Hawker, C. J. *Adv. Polym. Sci.* **1999**, *147*, 113
(23) Zeng, F.; Zimmerman, S. C. *Chem. Rev.* **1997**, *97*, 1681.
(24) Ignat′eva, G. M.; Rebrov, E. A.; Myakushev, V. D.; Chenskaya, T. B.; Muzafarov, A. M. *J. Polym. Sci., Part A* **1997**, *39*, 843.
(25) Majoral, J. P.; Caminade, A. M. *Top. Curr. Chem.* **1998**, *197*, 79.
(26) Bosman, A. W.; Jansen, H. M.; Meijer, E. W. *Chem. Rev.* **1999**, *99*, 1665.
(27) Gauthier, M.; Möller, M. *Macromolecules* **1991**, *24*, 4548.
(28) Tomaila, D. A.; Hedstrand, D. H.; Ferrito, M. S. *Macromolecules* **1991**, *24*, 1435.
(29) Jean-Luc, S.; Gnanou, Y. *Macromol. Symp.* **1995**, *95*, 137.
(30) Gauthier, M.; Tichagwa, L.; Downey, J. S.; Gao, S. *Macromolecules* **1996**, *29*, 519.
(31) Taton, D.; Cloutet, E.; Gnanou, Y. *Macromol. Chem. Phys.* **1998**, *199*, 2501.
(32) Wu, J.; Lieser, G.; Wegner, G. *Adv. Mater.* **1996**, *8*, 151.
(33) Cao, Y.; Smith, P. *Polymer* **1993**, *34*, 3139.
(34) Ito, K.; Kawaguchi, S. *Adv. Polym. Sci.* **1999**, *142*, 129.
(35) Tsukahara, Y.; Tsutsumi, K.; Yamashita, Y.; Shimada S. *Macromolecules* **1990**, *23*, 5201.
(36) Wintermantel, M.; Gerle, M.; Fischer, K.; Schmidt, M.; Wataoka, I.; Urakawa, H.; Kajiwara, K.; Tsukahara, Y. *Macromolecules* **1996**, *29*, 978.
(37) Ruokolainen, J.; Torkkeli, M.; Serimaa, R.; Vahvaselkä, S.; Saariaho, M.; ten Brinke, G. *Macromolecules* **1996**, *29*, 6621.
(38) Beers, K. L.; Gaynor, S. G.; Matyjaszewski, K.; Sheiko, S. S.; Möller, M. *Macromolecules* **1998**, *31*, 9413.
(39) Schappacher, M.; Deffieux, A. *Macromolecules* **2000**, 33, 7371.
(40) O′Donnell, P. M.; Brzezinska, K.; Wagener, K. B *Polym. Prepr. (Am. Chem. Soc., Div. Polym. Chem)* **1999**, *40*(2), 138.
(41) Percec, V.; Ahn, C.-H.; Ungar, G.; Yeardley, D. J. P.;. Möller, M.; Sheiko, S. S. *Nature* **1998**, *161*, 391.
(42) Percec, V.; Ahn, C.-H.; Cho, W.-D.; Jamieson, A. M.; Kim, J.; Leman, T.; Schmidt, M.; Gerle, M.; Möller, M.; Prokhorova, S. A.; Sheiko, S. S.; Cheng, S. Z. D.; Zhang, A.; Ungar, G.; Yeardley, D. J. P. *J. Am. Chem. Soc.* **1998**, *120*, 8619.
(43) Holerca, M. N.; Percec, V. *Biomacromolecules* **2000**, *1*, 6.
(44) Bo, Z.; Zhang, C.; Severin, N.; Rabe, J. P.; Schlüter, A. D. *Macromolecules* **2000**, *33*, 2688.
(45) Yin, R.; Zhu, Y.; Tomalia, D. A. *J. Am. Chem. Soc.* **1998**, *120*, 2678.
(46) Jahromi, S.; Coussens, B.; Meijerink, N.; Braam, A. W. M. *J. Am. Chem. Soc.* **1998**, *120*, 9753.
(47) Wang, P. W.; Liu, Y. J.; Devadoss, C.; Bharathi, P.; Moore, J. S. *Adv. Mater.* **1996**, *8*, 237.
(48) Zhao, M.; Crooks, R. M. *Adv. Mater.* **1996,** *11*, 217.
(49) Albrecht, M.; van Koten, G. *Adv. Mater.* **1996,** *11*, 171.
(50) Vasilenko, N. G.; Rebrov, E. A.; Muzafarov, A. M.; Esswein, B.; Striegel, B.; Möller, M. *Macromol. Chem. Phys* **1998**, *199*, 889.
(51) Leduc, M. R.; Hawker, C. J.; Dao, J.; Frechet, J. M. J. *J. Am. Chem. Soc.* **1996**, *118*, 11111.
(52) Zimmerman, S. C. *Curr. Opin. Colloid Interface Sci.* **1997**, *2*, 89.
(53) Cooper, A. J.; Londono, J. D.; Wignall, G.; McClain, J. B.; Samulski, E. T.; Lin, J. S.; Dobrynin, A.; Rubinstein, M.; Burke, A. L. C.; Frechet, J. M. J. *Nature* **1997**, *389*, 368.
(54) Jansen, J. F. G. A.; de Brabander-van der Berg, E. M. M.; Meijer, E. W. *Science* **1994**, *266*, 1226. Jansen, J. F. G. A.; de Brabander-van der Berg, E. M. M.; Meijer, E. W. *J. Am. Chem. Soc.* **1995**, *117*, 4417. Jansen, J. F. G. A.; de Brabander-van der Berg, E. M. M.; Meijer, E. W. *J. Am. Chem. Soc.* **1996**, *118*, 7398.
(55) Archut, A.; Vögtle, F.; Decola, L.; Azzellini, G. C.; Balzani, V.; Ramanujam P. S.; Berg R. H. *Chem. Eur. J.* **1996**, *4*, 699.
(56) Goino, M.; Esumi, K. *J. Colloid Interface Sci.* **1998**, 203, 214. Esumi, K.; Suzuki, A.; Aihara, N.; Usui K.; Torigoe, K. *Langmuir* **1998**, *14*, 3157.
(57) Jiang, D.-L.; Aida, T. *Nature* **1997**, *388*, 454.
(58) Junge, D. M.; McGrath, D. V. *J. Am. Chem. Soc.* **1999**, *121*, 4912.
(59) Larre, C.; Donnadieu, B.; Caminade, A. M.; Majoral, J. P. *Chem. Eur. J.* **1998**, *4*, 2031.
(60) Lorenz, K.; Hölter, D.; Stühn, B.; Mülhaupt, R.; Frey, H. *Adv. Mater.* **1996**, *8*, 414.
(61) Richardson, R. M.; Ponomarenko, S. A.; Boiko, N. I.; Shibaev, V. P. *Liq. Cryst.* **1999**, *26*, 101.
(62) van Hest, J. C. M.; Delnoye, D. A. P.; Baars, M. W. P. L.; van Genderen, M. H. P.; Meijer, E. W. *Science* **1999**, 268, 1592. Peerlings, H. W. I.; Meijer, E. W. *Chem. Eur. J.* **1997**, *3*, 1563.
(63) Bao, Z.; Amundson, K. R.; Lovinger, A. J. *Macromolecules* **1998**, *31*, 8647.
(64) Smith, S. B.; Finzi, L.; Bustamante, C. *Science* **1992**, *258*, 1122.
(65) Perkins, T. T.; Quake, S. R.; Smith, D. E.; Chu, S. *Science* **1994**, *264*, 822.
(66) Wang, M. D.; Yin, H.; Landick, R.; Gelles, J.; Block, S. M. *Biophys. J.* **1997**, *72*, 1335.
(67) Baumann, C. G.; Smith, S. B.; Bloomfield, V. A.; Bustamante, C. *Proc. Natl. Acad. Sci.* **1997**, *94*, 6185.
(68) Maier, B.; Strick, T. R.; Croquitte, V.; Bensimon, D. *Single Mol.* **2000**, *1*, 145.
(69) Wirtz, D. *Phys. Rev. Lett.* **1995**, *75*, 2436.
(70) Ziemann, F.; Rädler, J.; Sackmann, E. *Biophys. J.* **1994**, *66*, 2210.
(71) Furst, E. M.; Gast, A. P. *Phys. Rev. Lett.* **1999**, *82*, 4130.
(72) Merkel, R.; Nassoy; P.; Leung, A.; Ritchie, K.; Evans, E. *Nature* **1999**, *397*, 50.
(73) Cluzel, P.; Lebrun, A.; Heller, C.; Lavery, R.; Viovy, J.-L.; Chatenay, D.; Caron, F. *Science* **1996**, *271*, 792.
(74) Ishijima, A.; Kojima, H.; Higuchi, H.; Harada, Y.; Funatsu, T.; Yanagida, T. *Biophys. J.* **1996**, *70*, 383.
(75) Perkins, T. T.; Smith, D. E.; Larson, R. G.; Chu, S. *Science* **1995**, *268*, 83.
(76) Schurr, J. M.; Smith, S. B. *Macromolecules* **1990**, *29*, 1161.
(77) Long, D.; Viovy, J.-L.; Ajdari, A. *Biopolymers* **1996**, *39*, 755.
(78) Kumaki, J.; Nishikawa, Y.; Hashimoto, T. *J. Am. Chem Soc.* **1996**, *118*, 3321.
(79) Rivetti, C.; Guthold, M.; Bustamante, C. *J. Mol. Biol.* **1996**, *264*, 919.
(80) Sheiko, S. S. *Adv. Polym. Sci* **1999**, *151*, 61.
(81) Rabe, J. P. *Curr. Opin. Colloid Interface Sci.* **1998**, *3*, 27.

(82) Anselmetti, D.; Fritz, J.; Smith, B.; Fernandez-Busquets, X. *Single Mol.* **2000**, *1*, 53.
(83) Han, W.; Lindsay, S. M. *Nature* **1997**, *386*, 563.
(84) Hansma, H. G.; Vesenka, J.; Siegerist, C.; Kelderman, G.; Morrett, H.; Sinsheimer, R. L.; Elings, V.; Bustamante, C.; Hansma, P. K. *Science* **1992**, *256*, 1180.
(85) Rief, M.; Gautel, M.; Oesterhelt, F.; Fernandez, J. M.; Gaub, H. E. *Science* **1997**, *276*, 1109.
(86) Aimé, J. P.; Gauthier, S. In *Scanning Probe Microscopy of Polymers*; Ratner, B. D., Tsukruk, V. V., Eds.; ACS Symposium Series 694; American Chemical Society: Washington, DC, 1998.
(87) Leuba, S. H.; Zlatanova, J.; Karymov, M. A.; Bash, R.; Liu, Y.-Z.; Lohr, D.; Harrington, R. E.; Lindsay, S. M. *Single Mol.* **2000**, *1*, 185.
(88) De Paris, R.; Strunz, T.; Oroszlan, K.; Güntherodt, H.-J.; Hegner, M. *Single Mol.* **2000**, *1*, 285.
(89) Yamamoto, S.; Tsujii, Y.; Fukuda, T. *Macromolecules* **2000**, *33*, 5995.
(90) Hadziioannou, G.; Ortiz, C. *Macromolecules* **1999**, *32*, 780.
(91) Kudera, M.; Gaub, H. E. *Langmuir* **2000**, *16*, 4305.
(92) Furukawa, K.; Ebata, K.; Matsumoto, N. *Appl. Phys. Lett.* **1999**, *75*, 781.
(93) Lee, G. U.; Chrisey, L. A.; Colton, R. J. *Science* **1994**, *266*, 771.
(94) Chatellier, X.; Senden, T. J.; Joanny, J.-F.; di Meglio, J.-M. *Europhys. Lett.* **1998**, *41*, 303.
(95) Binnig, G.; Rohrer, H.; Gerber, Ch.; Weibel, E. *Phys. Rev. Lett.* **1982**, *49*, 57.
(96) Binnig, G.; Quate, C. F.; Gerber, Ch. *Phys. Rev. Lett.* **1986**, *56*, 930.
(97) *Procedures in scanning probe microscopies*; Colton, R. J., Engel, A., Frommer, J. E., Gaub, H. E., Gewirth, A. A., Guckenberger, R., Rabe, J., Heckl, W. M., Parkinson, B., Eds.; John Wiley & Sons: Chichester, 1998.
(98) Magonov, S. N.; Whangbo, M.-H. *Surface analysis with STM and AFM*; VCH Publishers: Weinheim, 1996.
(99) Tsukruk, V. V. *Rubber Chem. Technol.* **1997**, *70*, 430.
(100) Kajiyama, T.; Tanaka, K.; Ge, S.-R.; Takahara, A. T. *Prog. Surf. Sci.* **1996**, *52*, 1.
(101) Akari, S.; Horn, D.; Keller, W.; Schrepp, W. *Adv. Mater.* **1995**, *7*, 549.
(102) Noy, A.; Sanders, C. H.; Vezenov, D. V.; Wong, S. S.; Lieber, C. M. *Langmuir* **1998**, *14*, 1508.
(103) Thomas, R. C.; Tangyunyoung, P.; Houston, J. E.; Michalske, T. A.; Crooks. R. M. *J. Phys. Chem.* **1994**, *98*, 4493.
(104) Overney, R. M.; Meyer, E.; Frommer, J. E.; Brodbeck, D.; Lüthi, R.; Howald, L.; Güntherodt, H.-J.; Fujihira, M.; Takano, H.; Gotoh, Y. *Nature* **1992**, *359*, 133.
(105) Manne, S.; Gaub, H. E. *Curr. Opin. Colloid Interface Sci.* **1997,** *2*, 145.
(106) Wahl, K. J.; Stepnowski, S. V.; Unertl, W. N. *Tribol. Lett.* **1998**, *5*, 103.
(107) Overney, R. M. *Trends Polym. Sci.* **1995**, *3*, 359.
(108) Burnham, N. A.; Kulik, A. J.; Gremaud, G.; Gallo, P.-J.; Oulevey, F. *J. Vac. Sci. Technol. B* **1996**, *14*, 794.
(109) Rosa, A.; Weilandt, E.; Hild, S.; Marti, O. *Meas. Sci. Technol.* **1997**, *8*, 1.
(110) Bustamante, C.; Rivetti, C. *Annu. Rev. Biophys. Struct.* **1996**, *25*, 395.
(111) Bustamante, C.; Keller, D.; Yang, G. *Curr. Opin. Struct. Biol.* **1993**, *3*, 363.
(112) Lyubchenko, Y. L.; Oden, P. I.; Lampner, D.; Lindsay, S. M.; Dunker, K. A. *Nucleic Acids Res.* **1993**, *21*, 1117.
(113) Schaper, A.; Starink, J. P.; Jovin, T. M. *FEBS Lett.* **1994**, *355*, 91.
(114) Hansma, H. G.; Bezanilla, M.; Zenhausern, F.; Adrian, M.; Sinsheimer, R. L. *Nucleic Acids Res.* **1993**, *21*, 505.
(115) Zenhausern, F.; Adrian, M.; ten Heggeler-Bordier, B.; Eng, L. M.; Descouts, P. *Scanning* **1992**, *14*, 212.
(116) Hansma, H. G.; Vesenka, J.; Siegerist, C.; Kelderman, G.; Morrett, H.; Sinsheimer, R. L.; Elings, V.; Bustamante, C.; Hansma, P. K. *Science* **1992**, *256*, 1180.
(117) Yang, G.; Vesenka, J. P.; Bustamante, C. J. *Scanning* **1996**, *18*, 344.
(118) Hansma, H. G.; Sinsheimer, R. L.; Groppe, J.; Bruice, T. C.; Elings, V.; Gurley, G.; Bezanilla, M.; Mastrangelo, I. A.; Hough, P. V. C.; Hansma, P. K. *Scanning* **1993**, *15*, 296.
(119) Zhong, Q.; Innis, D.; Kjoller, K.; Elings, V. B. *Surf. Sci. Lett.* **1993**, *290*, L688:
(120) Leuba, S.; Yang, G.; Robert, C.; Samorí, B.; van Holde, K.; Zlatanova, J.; Bustamante, C. *Proc. Natl. Acad. Sci. U.S.A.* **1994**, *91*, 11621.
(121) Han, W.; Lindsay, S. M. *Nature* **1997**, *386*, 563.
(122) Hallett; P.; Tskhovrebova, L.; Trinick, J.; Offer, G.; Miles, M. J. *J. Vac. Sci. Technol. B* **1996**, *14*, 1444.
(123) Chu, S. *Science* **1991**, *253*, 861.
(124) Perkins, T. T.; Smith, D. E.; Larson, R. G.; Chu, S. *Science* **1995**, *268*, 83.
(125) Käs, J.; Strey, H.; Sackmann, E.. *Nature* **1994**, *268*, 226.
(126) Bustamante, C. *Annu. Rev. Biophys. Biochem.* **1991**, *20*, 415.
(127) Tinnefeld, P.; Buschmann, V.; Herten, D.-P.; Han, K.-T.; Sauer, M. *Single Mol.* **2000**, *1*, 215.
(128) Trautman, J. K.; Macklin, J. J.; Brus, M. E.; Bezig, E. *Nature* **1994**, *380*, 451.
(129) Funatsu, T.; Harada, Y.; Tokunaga, M.; Yanagida, T. *Nature* **1995**, *374*, 555
(130) Schäfer, B.; Gemeinhardt, H.; Uhl, V.; Greulich, K. O. *Single Mol.* **2000**, *1*, 33.
(131) Cornelissen, J. J. L. M.; Graswinckel, W. S.; Rowan, A. E.; Sommerdijk, N. A. J. M.; Nolte, R. J. M. *Polym. Prepr.* **2000**, *41* (1), 953.
(132) Falvo, M. R.; Clary, G. J.; Taylor, R. M., II; Chi, V.; Brooks; F. P., Jr.; Washburn, S.; Superfine, R. *Nature* **1997**, *389*, 582.
(133) Ponomarenko, S. A.; Boiko, N. T.; Zhu, X. M.; Agina, E. V.; Shibaev, V. P.; Magonov, S. N. *J. Polym. Sci., Part A* **2001**, *43*, 247.
(134) de Gennes, P. G. *Scaling Concepts in Polymer Physics*; Cornell University Press: Ithaca, NY, 1979.
(135) Landau, L. D.; Lifshitz, E. M. *Statistical Physics, Part 1*, 3rd ed; Pergamon Press: Oxford, New York, 1980.
(136) Schellman, J. A. *Biopolymers* **1974**, *13*, 217.
(137) Grosberg, A. Y.; Khokhlov, A. R. *Statistical Physics of Macromolecules*; API Press: Woodbury, NY, 1994.
(138) Kratky, O.; Porod, G. *Recueil* **1949**, *68*, 1106.
(139) Vasquez, C.; Kleinschmidt, A. K. *J. Mol. Biol.* **1968,** *34*, 137.
(140) Maier, B.; Rädler, J. O. *Macromolecules* **2000**, *33*, 7185.
(141) Edwards, S. F. *Proc. Phys. Soc. London* **1965**, *85*, 613.
(142) Smith, D. E.; Perkins, T. T.; Chu, S. *Macromolecules* **1996**, *29*, 1372.
(143) Rabe, J. P.; Buchholz, S. *Phys. Rev. Lett.* **1991**, *66*, 2096.
(144) Wavkuschewskij, A.; Cantow, H.-J.; Magonov, S. N.; Möller, M.; Liany, W.; Whanbo, M.-H. *Adv. Mater.* **1995**, *5*, 821.
(145) Mena-Osteritz, E.; Bäuerle, P. *Angew. Chem.. Int. Ed.* **2000**, *39*, 2679.
(146) Prokhorova, S. A.; Sheiko, S. S.; Möller, M.; Ahn, C.-H.; Percec, V. *Macromol. Rapid. Commun.* **1998**, *19*, 359.
(147) Prokhorova, S. A.; Sheiko, S. S.; Möller, M.; Ahn, C.-H.; Percec, V. *Macromolecules* **1998,** *32*, 2653.
(148) Prokhorova, S. A.; Sheiko, S. S.; Mourran, A.; Semenov, A. E.; Möller, M.; Beginn, U.; Zipp, G.; Ahn, C.-H.; Percec, V. *Langmuir* **2000**, *16*, 6862.
(149) Balagurusamy, V. S. K.; Ungar, G.; Percec, V.; Johansson, G. *J. Am. Chem. Soc.* **1997**, *119*, 1539.
(150) Kralchevsky, P. A.; Nagayama, K. *Langmuir* **1994**, *10*, 0¸23.
(151) Gerle, M.; Fischer, K.; Schmidt, M.; Roos, S.; Müller, A. H. E.; Sheiko, S. S.; Prokhorova, S. A.; Möller, M. *Macromolecules* **1999**, *32*, 2629.
(152) Sheiko, S. S.; Möller, M.; Reuvekamp, E. M. C. M.; Zandbergen, H. W. *Ultramicroscopy* **1994**, *53*, 371. Neves, B. R. A.; Vilela, J. M. C.; Russell, P. E. *Ultramicroscopy* **1999,** *76*, 61.
(153) Elbaum, M.; Fygenson, D. K.; Libchaber, A. *Phys. Rev. Lett.* **1996**, *76*, 4078.
(154) Lourie, O.; Cox, D. M.; Wagner, H. D. *Phys. Rev. Lett.* **1998**, *81*, 1638.
(155) Huck, W. T. S.; Bowden, N.; Onck, P.; Pardoen, T.; Hutchinson, J. W.; Whitesides, G. M. *Langmuir* **2000**, *16*, 3497.
(156) Sheiko, S. S.; Borisov, O. V.; Prokhorova, S. A.; Schmidt, U.; Möller, M.; Schmidt, M. Manuscript in preparation.
(157) Birshtein, T. M.; Borisov, O. V.; Zhulina, E. B.; Khokhlov, A. R.; Yurasova, T. A. *Polym. Sci. USSR* **1987**, *29*, 1293.
(158) Rouault, Y.; Borisov, O. V. *Macromolecules* **1996**, *29*, 2605.
(159) Williams, D. R. M. *Macromolecules* **1993**, *26*, 6667.
(160) Kwon, Y. K.; Chvalun, S. N.; Schneider, A. I.; Blackwell, J.; Percec, V.; Heck, J. A. *Macromolecules* **1994**, *27*, 6129.
(161) Strick, T. R.; Allemand, J.-F.; Bensimon, D.; Croquette, V. *Biophys. J.* **1998**, *74*, 2016.
(162) Marko, J. F.; Siggia, E. D. *Science* **1994**, *265*, 506.
(163) Marko, J. F.; Siggia, E. D. *Phys. Rev. E* **1995**, *52*, 2912.
(164) McLeish, T. *Science* **1997**, *278*, 1577.
(165) Khalatur, P. G.; Khokhlov, A. R.; Prokhorova, S. A.; Sheiko, S. S.; Möller, M.; Reineker, P.; Shirvanyanz, D. G.; Starovoitova, N. *Eur. Phys. J.* **2000**, *1*, 99
(166) Potemkin, I. I.; Khokhlov, A. R.; Reineker, P. *Eur. Phys. J.* **2001**, *4*, 93.
(167) Potemkin, I. I.; Sheiko, S. S.; Khokhlov, A. R.; Möller, M. Manuscript in preparation.
(168) Sheiko, S. S.; Prokhorova, S. A.; Beers, K. L.; Matyjaszewski, K.; Potemkin, I. I.; Khokhlov, A. R.; Möller, M. *Macromolecules* **2001**, *34*, 8354.
(169) Börner, H. G.; Beers, K.; Matyjaszewski, K.; Sheiko, S. S.; Möller, M. *Macromolecules* **2001**, *34*, 4375.
(170) Lifshitz, I. M.; Grosberg, A. Yu.; Khokhlov, A. R. *Rev. Mod. Phys.* **1978**, *50*, 683.
(171) Swislow, G.; Sun, S.-T.; Nishio, I.; Tanaka, T. *Phys. Rev. Lett.* **1980**, *44*, 796.
(172) Rark, I. M.; Wang, Q.-W.; Chu, B. *Macromolecules* **1987**, *20*, 1965.
(173) Ueda, M.; Yoshikawa, K. *Phys. Rev. Lett.* **1996**¸*77*, 2133.

(174) Yoshikawa, K.; Takahashi, M.; Vasilevskaya, V. V.; Khokhlov, A. R. *Phys. Rev. Lett.* **1996,** *76*, 3029.
(175) Tokuhisa, H.; Zhao, M.; Baker, L. A.; Phan, V. T.; Dermody, D. L.; Garcoa, M. E.; Peez, R. F.; Crooks, R. M.; Mayer, T. M. *J. Am. Chem. Soc.* **1998**, *120*, 4492.
(176) Sheiko, S. S.; Buzin, A. I.; Muzafarov, A. M.; Rebrov, E. A.; Getmanova, E. V. *Langmuir* **1998**, *14*, 7468.
(177) Li, S.; Hanley, S; Khan, I.; Varshney, S. K.; Eisenberg, A.; Lennox, R. B. *Langmuir* **1997**, *9*, 2243
(178) Li, Z.; Zhao, W.; Rafailovich, M. H.; Sokolov, J.; Lennox, R. B.; Eisenberg, A.; Wu, X. Z.; Kim, M. W.; Sinha, S. K.; Tolan, M. *Langmuir* **1995**, *11*, 4785.
(179) Bloom, G. S.; Endow, S. A. *Protein Profile* **1995**, *2*, 1105.
(180) Barton, N. R.; Goldstein, L. S. *Proc. Natl. Acad. Sci.* **1996**, *93*, 1735.
(181) Mooseker, M. S.; Cheney, R. E. *Annu. Rev. Cell Dev. Biol.* **1995**, *11*, 633.
(182) Sellers, J. R.; Goodson, H. V. *Protein Profile* **1995**, *2*, 1323.
(183) Gibbons, B. H.; Asaj, D. J.; Tang, W.-J. Y.; Hays, T. S.; Gibbons, I. R. *Mol. Biol. Cell.* **1994**, *5*, 57.
(184) Spudich, J. A. *Nature* **1994**, *372*, 515.
(185) Kitamura, K.; Tokunaga, M.; Iwane, A. H.; Yanagida, T. A. *Nature* **1999**, *397*, 129.
(186) Adjari, A.; Prost, J. *C. R. Acad. Sci. Paris* **1993**, *II 315*, 1635.
(187) Muthukumar, M. *J. Chem. Phys.* **1985**, *82*, 5696
(188) Komura, S.; Seki, K. *J. Phys. II* **1995**, *5*, 5.
(189) Doi. M.; Edwards, S. *The Theory of Polymer Dynamics*; Clarendon: Oxford 1986; p 100.
(190) Tartsch, B.; Prokhorova, S.; Sheiko, S. S.; Holcera, M. N.; Percec, V., Möller, M. Manuscript in preparation.

CR990129V